A very large Xenon double-beta decay experiment

Opportunities in science, technology and nuclear non-proliferation

R. DeVoe[3], A. Dolgolenko[4], G. Giannini[11], G. Gratta[8], P. Picchi[5,9,10], A. Piepke[1], F. Pietropaolo[7], J-L. Vuilleumier[6], P. Vogel[2], Y-F. Wang[8], O. Zeldovich[4]

[1] *Physics Department, University of Alabama, Tuscaloosa AL*
[2] *Bridge Laboratory, Caltech, Pasadena CA*
[3] *Almaden Research Center, IBM, San Jose CA*
[4] *ITEP, Moscow, Russia*
[5] *INFN, Laboratori Nazionali di Frascati, Italy*
[6] *Institut de Physique, Universite de Neuchatel, Switzerland*
[7] *INFN, Sezione di Padova, via Marzolo 8, Padova, Italy*
[8] *Physics Department, Stanford University, Stanford CA*
[9] *Istituto di Cosmogeofisica del CNR, Torino, Italy*
[10] *Dipartimento di Fisica, Università di Torino, Italy*
[11] *Dipartimento di Fisica, Università di Trieste, Italy*

September 1999

Contents

1 Overview **5**

2 Physics Considerations **7**
- 2.1 Survey of neutrino physics 7
- 2.2 Cosmological implications 12
- 2.3 Double-beta decay 12
- 2.4 Present status of $0\nu\beta\beta$ decay searches 16

3 Detector design concepts **21**
- 3.1 A large Xe gas TPC 22
  - 3.1.1 Chamber Layout 24
  - 3.1.2 Gas System 27
  - 3.1.3 Readout System 30
- 3.2 Barium spectroscopy and atom tagging 32
  - 3.2.1 Laser Detection of Single Atoms in Atomic Physics 32
  - 3.2.2 Barium Detection in High Pressure Xenon 33
  - 3.2.3 Laser Detection System 35
  - 3.2.4 Possible Applications of Atom Tagging at High Pressures . . . 36
- 3.3 Estimated Detector Performance 36

4 Xenon Enrichment Program **40**
- 4.1 Enrichment Requirements and Techniques 40
- 4.2 Nuclear Non-proliferation Issues 43

5 Acknowledgments **46**

1 Overview

The progress of fundamental science and technology and their interaction with our society are often intertwined in a surprising fashion, with contributions to each field coming from seemingly unrelated directions. Such symbiosis among human activities naturally leads to fundamental scientific discoveries, that result in unexpected technological advances that, in turn, improve our living standards and fuel new and more advanced discoveries. This development has remarkably few rules and surprises are the standard rewards.

In a different sphere the advent of fast transportation, information technologies and weapons of mass destruction has linked previously disconnected geographical regions and interests around the world, so that in modern language, the term "society" used above refers more than ever to the population of the entire planet. While this global point of view is quite familiar within some scientific circles that have been sharing ideas on a planetary scale since the beginning of the century, only very recently the connections between science, technology and society are crossing the boundaries of continents.

In this document we will describe a program that would naturally marry research in some of the most fundamental field of science with state-of-the-art-technology and essential issues of nuclear non-proliferation. The quality of each facet of such program is first rate, while the different facets strictly depend on each other. There is no science without the technology and the non-proliferation sub-programs; the opportunity in non-proliferation relies on the science and technology; there could be new practical technologies emerging from the program.

The experiment described below involves a possible breakthrough in the study of neutrinos, the least known of the fundamental constituents of matter. The study of neutrinos has recently become a central issue in many disciplines of fundamental science, including particle physics, cosmology and astrophysics. While neutrinos have been used for many years as tools to investigate some of the fundamental forces of nature, only in the last few years we have seriously began to explore their fundamental properties. The principal result of such an effort is the tentative discovery [1, 2, 3, 4] that neutrinos do have a finite (albeit very small) mass. While a non-zero neutrino mass could essentially reshape the way we understand fundamental particles, their interactions and the development of our universe, our knowledge of neutrino masses relies on the phenomenon of neutrino oscillations that, as explained later, does not provide the absolute magnitude of the masses themselves.

It appears that in the near future the most likely source of information on such masses will be the hypothetical phenomenon of neutrinoless double-beta decay ("$0\nu\beta\beta$ " in short), whereby a nucleus would decay emitting two electrons and no neutrinos. The rate of occurrence of such process can be related to a neutrino mass. Several experiments have been conducted in the past to search for such process always with negative results, providing upper-limits to neutrino masses. In order to extend

this study beyond such limits (and into the regime interesting for the modern hints to masses) a substantial step in sensitivity is required. Searches for $0\nu\beta\beta$ -decay need to be performed using several *tons* of an appropriate isotope while maintaining the ability to observe a signal of few events per year with negligible background.

We will show here that a new technique involving the tagging with optical spectroscopy of single atoms of the decay product can be used today to produce background-free measurements. The only isotope that can be used in this fashion is ^{136}Xe that is a noble gas at standard conditions and would transmute through $\beta\beta$ decay into a barium ion. The technology for optically tagging barium ions has been extensively developed (for different purposes) in the last several years. The development of this spectroscopic technique for the high pressure environment required for the experiment may have useful technological applications in the future.

The feasibility of such an experiment entirely relies on the procurement of very large amounts of enriched ^{136}Xe . This isotope is particularly easy to enrich (from the $\simeq 9\%$ content of natural xenon) with a number of methods and, particularly, ultra-centrifugation. A program of enrichment capable of producing tons of ^{136}Xe could be practically carried on at a large military enrichment facility in Russia, hence at the same time providing civilian work for sensitive personnel and equipment. The purity and cleanliness requirements for this program would naturally require strict quality control and serve as training towards a reconversion of the laboratory towards further civilian and commercial ventures. In addition such production would ideally match the expertise of the scientists and engineers involved, providing a stimulating and worthwhile working environment. The involvement of US, European and Russian civilian scientists, accustomed to successfully collaborate in fundamental science, would provide a constructive base for future programs directed to the improvement of world security through the transformation of weapon facilities into a healthy community of civilian scientists and technologists.

2 Physics Considerations

2.1 Survey of neutrino physics

Neutrinos have the distinction of being the first elementary particles whose existence was predicted by a theorist in order to explain seemingly unrelated phenomena. Pauli made such prediction in 1930 in a famous letter in order to explain the continuous electron energy distribution in nuclear beta decay. It became immediately clear (thanks to Bethe and Peierls) that neutrinos will be difficult to observe, because the corresponding cross sections are so tiny. But in a series of experiments in 1953-56 Cowan, Reines and collaborators were able to prove convincingly that electron anti-neutrinos from nuclear reactors are able to cause the inverse neutron beta decay, $\bar{\nu}_{\rm e} + {\rm p} \rightarrow {\rm e}^+ + {\rm n}$, and hence that they are real particles. Shortly afterwards, in 1962, the separate identity of the muon neutrinos, ν_μ, was demonstrated. Another decade later, in 1975, the tau lepton was discovered by Perl *et al.*, and the observation of its decay properties implied the existence of the third neutrino, ν_τ. More recently the precise measurements of the decay width of the Z boson have shown that just three neutrino flavors participate in the weak interactions (at least for neutrinos with masses less than $M_{\rm Z}/2$).

Ironically, while our knowledge of intrinsic neutrino properties remains quite poor, these particles have been used as tools to elucidate other phenomena of nature. Thirty years ago Davis and his collaborators were first able to detect neutrinos from the Sun. This was, and still is, the only clear proof that the basic energy generation in stars is understood. Neutrino-induced reactions also played an important role in establishing what is now known as the Standard Model of electroweak interactions when in 1973 the neutral currents were discovered via the observation of the $\nu_\mu + {\rm e} \rightarrow \nu_\mu + {\rm e}$ scattering as well as the neutral current scattering of neutrinos on nucleons. Neutrinos have been extensively used in deep inelastic scattering experiments at CERN and FNAL, exploring the quark structure of nucleons. Finally neutrino astronomy was born with the observation of the neutrino burst from the supernova 1987A.

The main problem in neutrino physics today is the question whether neutrinos, like the charged fermions, have a mass. When the Standard Model of electroweak interactions was established, there was no experimental reason to introduce a neutrino mass, and hence the model postulated that neutrinos are massless. This assumption was consistent with the observation that the individual lepton flavors seem to be conserved (and, naturally, the total lepton number as well). In addition, since the upper limits on neutrino masses are so much smaller than the masses of the corresponding charged leptons (or quarks) it was "natural" to assume that, in fact, neutrinos are massless, hence avoiding the unnaturally small mass ratios. However, at present there is a consensus among theorists that the Standard Model cannot be applicable at arbitrarily high energies. Rather, most theorists consider the Standard Model an effective field theory which should be a good description of nature only up to some

energy limit where new physics will manifest itself. This point of view naturally leads to the expectation that neutrino masses acquire a value of the order $\langle\Phi\rangle^2/M$, where $\langle\Phi\rangle$ is the Higgs vacuum expectation value ($\approx$250 GeV), and M is the energy scale of new physics. As long as $\langle\Phi\rangle \ll M$ the neutrino masses will be naturally small.

One can come to a similar conclusion from a rather different viewpoint as well, as in the see-saw mechanism. Within the general framework of the Standard Model, one simply assumes the existence of new particles, the heavy neutrino electroweak singlets. The see-saw mechanism then results in the light Majorana neutrino mass of the order M_f^2/M_R, where M_f is the mass of a generic Dirac fermion (quark or lepton) and M_R is the mass of the heavy singlet neutrino. Again, as long as $\langle M_f\rangle \ll M_R$, physical neutrinos will be very light Majorana fermions. Thus, various reasonable extensions of the Standard Model typically predict the existence of neutrino mass. While mass values are not accurately predicted, it appears that with reasonable values of the large mass scales M and/or M_R neutrino masses in the 0.01 - 1 eV range are preferred, in agreement with the experimental hints described below. Most of such extensions, moreover, lead to the expectation that the massive neutrinos are Majorana particles, and that the phenomenon of mixing, analogous to the Cabibbo-Kobayashi-Maskawa mixing among quarks, will govern their weak interactions.

At present there is no well established, and independently confirmed evidence that the scenario sketched above exists in nature. Indeed it is true that any theoretical description of elementary particles and interactions fails to explain the masses *of all* the particles observed in nature. In other words, while we do not know for sure whether neutrino masses are zero or finite, in a broader sense we ignore what kind of mechanism assigns a mass to *any* particle. Therefore the study of neutrino masses plays a very central role in particle physics.

The results of a number of independent experiments [1, 2, 3] can be interpreted as due to finite neutrino masses and, most recently, high statistics measurements of atmospheric neutrinos by the Super-Kamiokande[4] experiment are regarded by most as firm evidence that neutrinos do have a non-zero mass.

Evidence for neutrino mass is being pursued in studies involving neutrinos created in astrophysical objects (Sun, supernovae), in the earth atmosphere, in accelerators and nuclear reactors, in weak decays of nuclei and elementary particles, and in studies of reactions and decays where neutrinos appear as virtual particles, such as the neutrino-less double beta decay. In the rest of this section we will review some of these techniques, while neutrino-less double beta decay will be discussed in a separate section.

Conceptually, the simplest way to search for the neutrino mass is based on the kinematic studies of the particles produced in weak decays such as $^3\mathrm{H} \rightarrow ^3\mathrm{He}\ \mathrm{e}^-\bar{\nu}_\mathrm{e}$, $\pi \rightarrow \mu\nu_\mu$ and $\tau \rightarrow n\pi\nu_\tau$. The latter two processes result in limits for the mass of ν_μ and ν_τ of, respectively, 170 keV and 18.2 MeV. The limit on the $\bar{\nu}_\mathrm{e}$ mass from the tritium beta decay, however, is in the few eV range. Unfortunately, the interpretation of the tritium beta decay experiments is plagued at the present time by (apparently)

systematic uncertainties leading to the best fit in the unphysical range $m_\nu^2 < 0$.

Another conceptually simple neutrino mass determination is based on the time-of-flight method with the supernova neutrinos. In particular, for a Galactic supernova, determining the time delay between the neutral current signal caused by the ν_μ and ν_τ neutrinos, and the charged current signal caused by the $\bar{\nu}_e$ neutrinos, one can reach sensitivities well below the above limits. Large underground detectors like KamLAND, LVD and Super-Kamiokande[5] will be particularly well equipped to perform such a measurement that, however, requires a supernova explosion in the right region of the universe.

The experimental hints for neutrino mass are at present based on the phenomenon of neutrino oscillations. If, as suggested above, neutrinos are massive particles which behave in analogy to quarks, the states with a definite mass (i.e., the "mass eigenstates" which propagate as plane waves in a vacuum) are not necessarily the partners of the charged leptons that couple to the vector bosons $W^\pm$ in doublets (i.e., the weak eigenstates)

$$\left(\begin{array}{c} \nu_{\rm e} \\ {\rm e}^- \end{array} \right) , \left(\begin{array}{c} \nu_\mu \\ \mu^- \end{array} \right) , \left(\begin{array}{c} \nu_\tau \\ \tau^- \end{array} \right) . \qquad (1)$$

The weak eigenstates $|\nu_l\rangle$ will be in such a case linear superpositions of the mass eigenstates $|\nu_i\rangle$

$$|\nu_l\rangle = \sum_i U_{l,i} |\nu_i\rangle \ , \qquad (2)$$

where the coefficients $U_{l,i}$ form the leptonic mixing matrix. If we assume that only three neutrinos can contribute in the Eq. (2) above, then U is a unitary 3×3 matrix.

If Eq. (2) is valid, we encounter the phenomenon of neutrino oscillations in which a neutrino which was initially in the weak eigenstate l can be spontaneously transformed, at least in part, into another weak eigenstate neutrino of flavor l'.

For a simplified two neutrino flavors mix, e.g. e and μ one finds that the mixing matrix U depends only on one mixing angle θ, and the oscillation probability is given by

$$U = \left(\begin{array}{cc} \cos\theta & \sin\theta \\ -\sin\theta & \cos\theta \end{array} \right) \ , \ P(\nu_{\rm e} \to \nu_\mu, L) = \sin^2 2\theta \, \sin^2(\Delta m^2 L/4E) \ . \qquad (3)$$

Here $\Delta m^2 \equiv m_1^2 - m_2^2$. The probability that $\nu_{\rm e}$ remains $\nu_{\rm e}$ is obviously $P(\nu_{\rm e} \to \nu_{\rm e}, L) = 1 - P(\nu_{\rm e} \to \nu_\mu, L)$.

Numerous searches for neutrino oscillations were performed during the last two decades. Most of them resulted in an "exclusion plot", i.e., based on them certain ranges of the parameters Δm^2 and $\sin^2 2\theta$ can be excluded from further considerations as shown in Figure 1. However, at the present time there are three groups of measurements that suggest the existence of neutrino oscillations. (And, at the same time, the parameter ranges suggested by them are not excluded.)

The first group of measurements which are interpreted as evidence for neutrino oscillations deals with the "missing" solar neutrinos. The Sun produces an intense

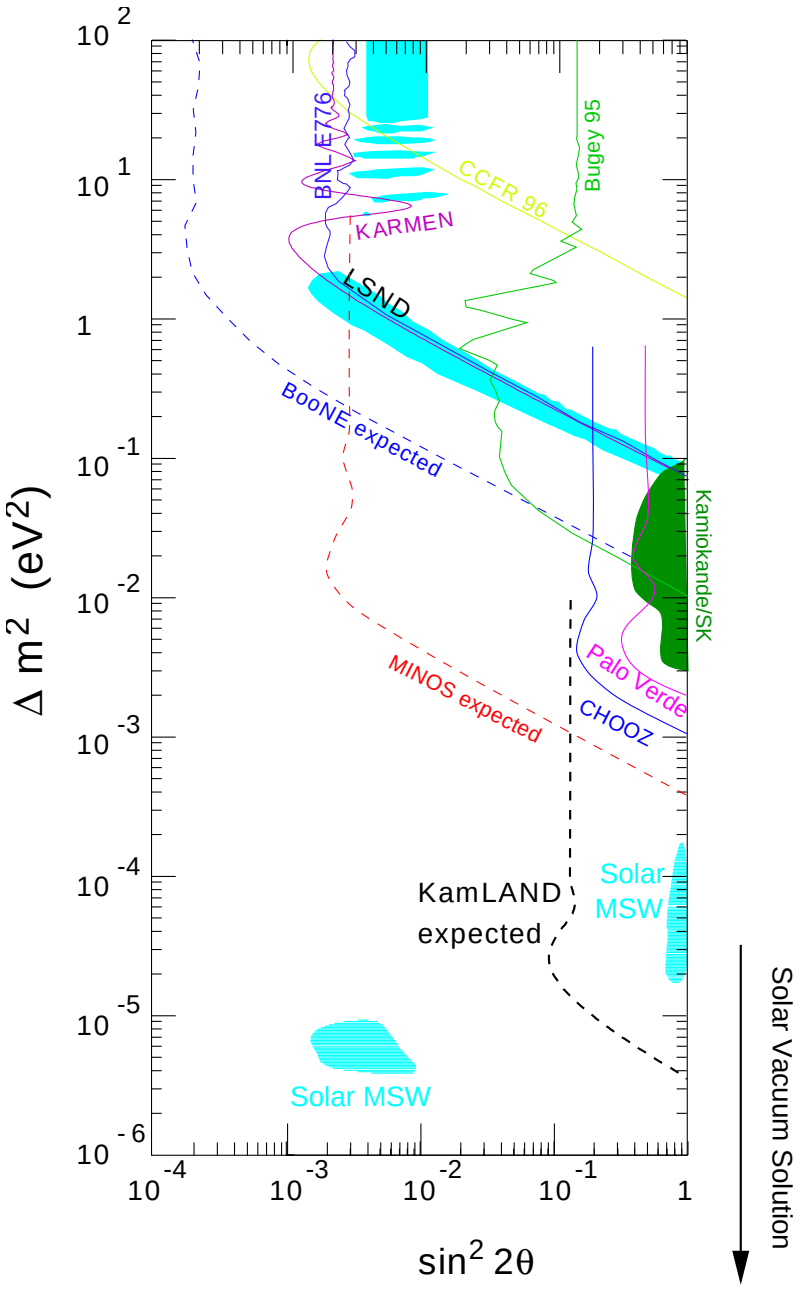

Figure 1: Parameter space for neutrino oscillations. Curves represent upper limits from different experiments (continuous curves are existing limits, dashed curves are projected for future experiments). Shaded areas represent the allowed regions obtained by interpreting solar, atmospheric and LSND anomalies as due to oscillation. All measurements are at 90% CL and while the exclusion curves refer to $\nu_e - \nu_X$ oscillations the allowed regions in this summary plot do not necessarily occur in the $\nu_e - \nu_X$ channel.

flux of electron neutrinos as a byproduct of the fusion reactions which generate solar power. It is believed that the solar structure is understood sufficiently well so that the flux and energy spectrum of the solar neutrinos can be confidently predicted. The solar neutrino fluxes have been measured in five experiments so far [3]. All of them report a deficit, i.e., the measured flux is less than the expected one. Moreover, the reduction depends on the neutrino energy, inferred experimentally from the thresholds of the individual detectors. The only viable explanation of the deficit appears to be neutrino oscillation ($\nu_{\rm e}$ disappearance). By contrast to the attempts to explain the deficit by modification of the solar model, which are unsuccessful, all existing data can be simply and elegantly explained by invoking neutrino mass. In particular, the solution based on the MSW effect[6] offers the most popular scenario. Treating the problem in the two-flavor framework explained above, one arrives at two isolated islands in the Δm^2 – $\sin^2 2\theta$ plane. Both solutions correspond to $\Delta m^2 \approx 10^{-5}$ eV^2. One of them has rather small $\sin^2 2\theta \approx 10^{-2}$. The other one has much larger mixing angle, $\sin^2 2\theta \geq 0.5$. This solution also spans a larger interval of Δm^2 extending up to 10^{-4} eV^2.

The second set of measurements that is today regarded as the most compelling evidence for neutrino oscillations is the "atmospheric neutrino anomaly" [1, 4]. Primary cosmic rays impinging on the nitrogen and oxygen nuclei at the top of the earth's atmosphere produce mostly pions, which subsequently decay via $\pi \to \mu\bar{\nu}_\mu, \mu \to {\rm e}\bar{\nu}_{\rm e}\nu_\mu$. The resulting atmospheric neutrinos therefore are expected to follow the $\nu_\mu : \nu_{\rm e} = 2:1$ ratio, which is essentially independent of the details of the complicated process that created them. In addition, in an underground detector, one can deduce the direction of the incoming neutrinos from the direction of the leptons (e and μ) created by the charged current interactions, at least at high enough energies. Again, one is reasonably confident that this zenith angle distribution can be accurately predicted. If the ν_μ and/or $\nu_{\rm e}$ neutrinos oscillate, one expects deviations from the 2:1 ratio mentioned above. Also, since the zenith angle is simply related to the neutrino path length, one expects deviations from the expected zenith angle dependence of the lepton yield.

Both signatures of neutrino oscillations were in fact observed. The ν_μ/ν_e ratio is noticeably smaller, only about 60% of the expected value of 2. This result has been confirmed in four detectors thus far. The anomalous zenith angle dependence was first observed in Kamiokande, and has been now confirmed, with much better statistical significance, by Super-Kamiokande. If these effects indeed signify neutrino oscillations (and we do not have another viable explanation) then the corresponding mixing angle is large, $\sin^2 2\theta \approx 1$. The value of the mass parameter Δm^2 remains uncertain, but is clearly in the range 10^{-2} - 10^{-4} eV^2. Super-Kamiokande data, along with the results from the Chooz [7] and Palo Verde [8] reactor experiments clearly prefer the scenario involving $\nu_\mu \to \nu_\tau$ oscillations.

Finally, the only indication for oscillations involving artificially-made neutrinos comes from the LSND experiment which finds evidence for the $\bar{\nu}_\mu \to \bar{\nu}_{\rm e}$ and, with more limited statistics, also for $\nu_\mu \to \nu_{\rm e}$ [2]. The former channel uses neutrinos from

the pion and muon decay at rest, with energies less than $m_\mu/2$. The latter channel uses neutrinos from the pion decay in flight which have somewhat higher energies. These are appearance experiments; the observed signal should be absent if neutrinos do not oscillate. The well determined quantity is the oscillation probability, which has the value of about 3×10^{-3}. This result has not been independently confirmed but it is not contradicted by other evidence either.

A summary of the tentative evidence for oscillations is also given in Figure 1. While the tentative conclusion is that oscillations do occur and, hence, neutrino masses are non-zero, only the parameter $\Delta m^2 = m_i^2 - m_j^2$ is measured with oscillations so that we have no knowledge of the individual mass value. In particular drastically different mass scenarios are still allowed by data. On one extreme neutrino masses could follow a hierarchical configuration, like in the case for charged leptons and quarks ($m_{\nu_e} < m_{\nu_\mu} < m_{\nu_\tau}$); while on the other we could easily envisage an almost degenerate situation where all neutrinos have masses that are much larger than the mass differences, like in the case of the $K^0 - \bar{K}^0$ system. Only a kinematics measurement or the observation of neutrino-less double beta decay can elucidate this important point.

2.2 Cosmological implications

Neutrino masses also play a remarkable role in cosmology. If neutrinos are stable, or at least have lifetimes longer than the age of the Universe ($\simeq 10^{10}$yr), one confidently expects the existence of a primordial neutrino sea, analogous to the well established 2.7 K background microwave radiation. As illustrated in Figure 2, while photons decoupled from matter $\sim 10^{12}$ s (30,000 years) after the big bang, neutrino decoupling occurred much earlier, about 1 s after the big bang. The corresponding temperature of today's sea of neutrino is 1.9 K, colder than in the case of photons. The number density of such relic neutrinos has been greatly reduced by the expansion of the universe and today it is estimated to amount to ~ 300 cm^{-3} including all neutrino flavors. If neutrinos are massive, then enough mass could be contained in the neutrino sea to account for (at least part of) the "dark matter" in the universe. Since the critical energy (or mass) density of the universe is $\rho_c \sim 5$ keVcm^{-3}, neutrino masses of up to 15 eV (mass average over the three flavors) could explain the majority of the mass in the universe. While it is generally accepted that, for a number of reasons, neutrinos alone cannot contribute more than a fraction of the critical density, the experimental observation of neutrino masses between few meV and few eV would have very significant consequences for cosmology and astrophysics.

2.3 Double-beta decay

Double beta decay is the transition between a nucleus of charge Z and mass number A (with A and Z both even) and one of same mass number but charge $Z+2$. Here

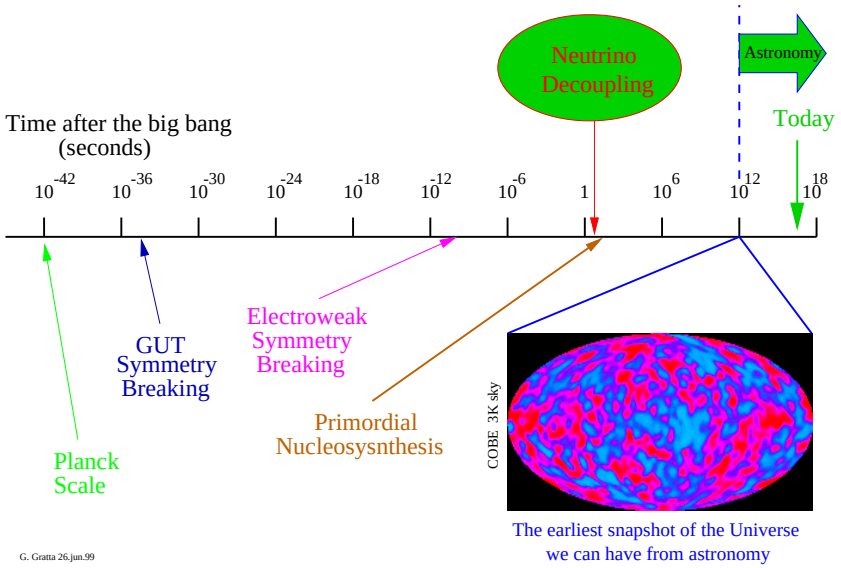

Figure 2: Photon and neutrino decoupling are shown in the time-development of the universe (time in seconds after the big bang.) Relic neutrinos, that decoupled from matter at $t \sim 1$ s, permeate today's universe with a number density of ~ 300 cm^{-3}. Massive neutrino could represent a substantial part of the "dark matter" in the universe.

we will limit ourselves to a review of results and problems, while a more complete treatment is given in several articles [9].

In its basic form ($2\nu\beta\beta$) double beta decay can be regarded as two β^- decays happening simultaneously from the point of view of the nuclear forces, so that the process

$$(Z, A) \rightarrow (Z + 2, A) + \mathrm{e}_1^- + \mathrm{e}_2^- + \bar{\nu}_{\mathrm{e}1} + \bar{\nu}_{\mathrm{e}2} \tag{4}$$

produces four leptons in the final state. While this second-order process is a rather standard manifestation of nuclear physics, its rate is expected to be proportional to $(G_F \cos\theta_C)^4$ where G_F is the Fermi coupling constant and θ_C the Cabibbo angle. Hence double beta decay would be an unobservably small correction to regular beta decay if it was not for a peculiarity in the nuclear mass function that in some cases renders the first order process (regular β^- decay) energetically disallowed. As shown in Figure 3 (for the case of A=136) odd-odd and even-even nuclei are arranged on two different mass parabolae because of the different value of the pairing term in the nuclear binding energy. While the direct β transition (^{136}Xe $\rightarrow^{136}$ Cs) is now forbidden, the double-β process is here energetically possible. Although this situation is rather common, only in 11 cases the kinetic energy available to the leptons (Q) is larger than 2 MeV so that the hypothetical double-β decay can be observed in good experimental conditions.

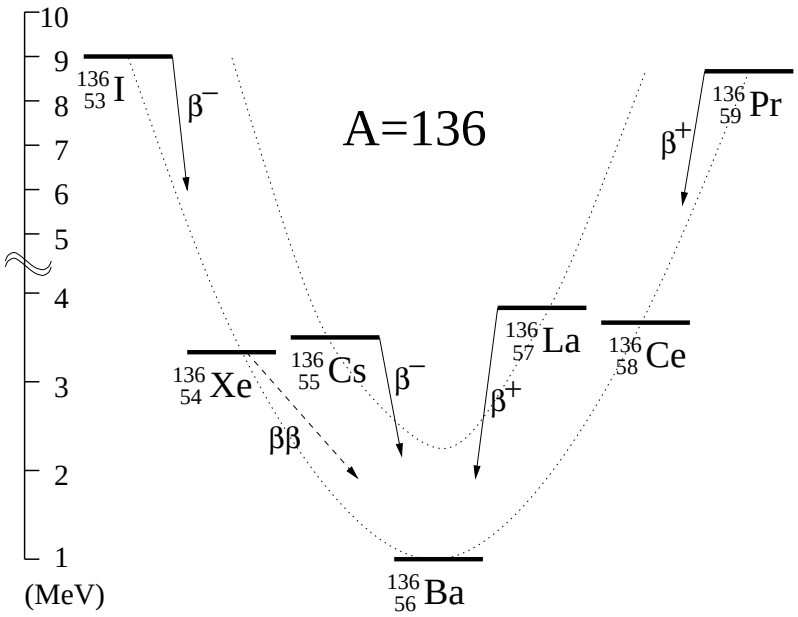

Figure 3: Simplified atomic mass scheme for nuclei with A=136. The parabolae connecting the odd-odd and even-even nuclei are shown. While ^{136}Xe is stable for ordinary β^- decay, it can decay into ^{136}Ba by a double-beta process.

For completeness we also mention here the processes

$$(Z, A) \rightarrow (Z-2, A) + \mathrm{e}_1^+ + \mathrm{e}_2^+ + \nu_{\mathrm{e}1} + \nu_{\mathrm{e}2} \tag{5}$$

$$(Z, A) + e_1^- \rightarrow (Z-2, A) + \mathrm{e}_2^+ + \nu_{\mathrm{e}1} + \nu_{\mathrm{e}2} \tag{6}$$

$$(Z, A) + e_1^- + e_2^- \rightarrow (Z-2, A) + \nu_{\mathrm{e}1} + \nu_{\mathrm{e}2} \tag{7}$$

analogous to β^+ decay and to (single or double) electron capture. Such processes may happen in nature but only in one case (^{124}Xe $\rightarrow^{124}$ Te) Q is above 1 MeV. Since the decay rates increase rapidly with Q we will concentrate on the case in Eq. 4.

$2\nu\beta\beta$ decay has been observed in some 11 different isotopes and the half life measured can be used to verify nuclear structure models in the presence of second order weak processes. Calculations in general agree quite well with measurements.

As illustrated in Figure 4 a different kind of double beta decay ($0\nu\beta\beta$) involving no neutrinos in the final state may occur if lepton number is not a conserved quantity *and* neutrinos have non-zero mass. Here the requirement of lepton number non-conservation derives from the fact that the anti-neutrino emitted in A has to be identical to a neutrino in order to be re-absorbed in B (Majorana neutrino). Furthermore, since weak interactions only couple to left-handed states, the neutrino has to have a mass in order not to be an eigenstate of helicity.

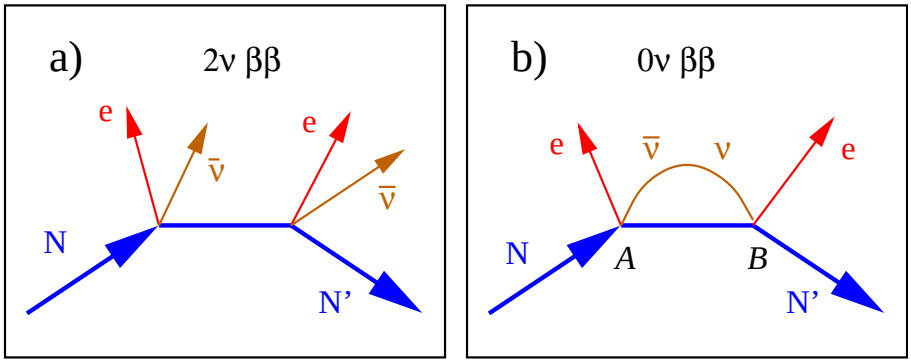

Figure 4: Feynman graphs relative to: a) 2-neutrino and (b) 0-neutrino double-beta decay processes.

In addition, if the lepton number non-conservation is due to a mechanism of spontaneous symmetry breaking, double beta decay could occur as

$$(Z, A) \rightarrow (Z + 2, A) + \mathrm{e}_1^- + \mathrm{e}_2^- + \chi \tag{8}$$

where the particle χ (Majoron) is the Goldstone boson of the lepton number symmetry breaking. In all models χ is a weakly interacting particle that cannot be detected.

While it is known [10] that new, exotic particles can be replaced for the neutrino in Figure 4b and produce $0\nu\beta\beta$, it is in general true that the observation of $0\nu\beta\beta$ would imply the discovery of previously unknown physics. Indeed the connection between neutrino masses or, in general, new physics beyond the "standard model" and the existence of $0\nu\beta\beta$ drives the interest for this process.

The decays $2\nu\beta\beta$, $0\nu\beta\beta$ and $\chi\beta\beta$ experimentally can only be differentiated from each other from the spectrum of the total electron energy in the final state as shown in Figure 5.

If the $0\nu\beta\beta$ process occurs, then the *effective* Majorana neutrino mass $\langle m_\nu \rangle$ is related to the half-life $T_{1/2}^{0\nu\beta\beta}$ as:

$$\langle m_\nu \rangle^2 = (T_{1/2}^{0\nu\beta\beta} G^{0\nu\beta\beta}(E_0, Z) |M_{GT}^{0\nu\beta\beta} - \frac{g_V^2}{g_A^2} M_F^{0\nu\beta\beta}|^2)^{-1} \tag{9}$$

where $G^{0\nu\beta\beta}(E_0, Z)$ is a phase space factor depending on the end-point energy E_0 and $M_{GT}^{0\nu\beta\beta}$ and $M_F^{0\nu\beta\beta}$ are the Gamow-Teller and Fermi nuclear matrix elements for the process. Here we have defined

$$\langle m_\nu \rangle = \sum_i m_i U_{ei}^2 \tag{10}$$

U being the mixing matrix in the lepton sector and m_i the masses of the individual Majorana neutrinos. Hence $0\nu\beta\beta$ decay is sensitive to the masses of all neutrino flavors, provided that the mixing angles are non-negligible.

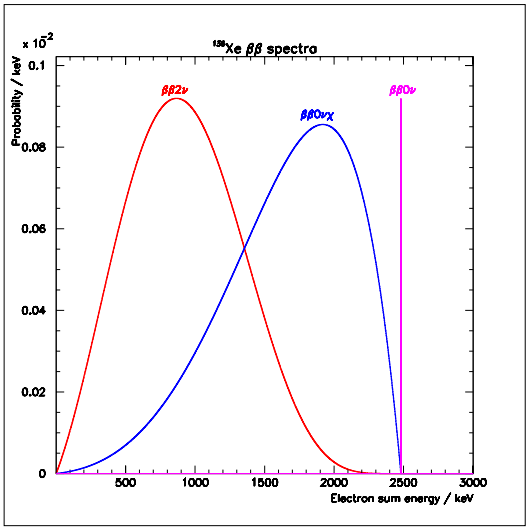

Figure 5: Spectra for the sum of electron energies in the final states for the three different ^{136}Xe $\beta\beta$ decay modes considered in the text. The relative amplitudes of the different curves are arbitrary. While the exact positions of the peaks in the spectra differ for various isotopes, the general features are obviously common to all $\beta\beta$ emitters.

From Equation 9 we find that the sensitivity to neutrino masses improves only with the square root of the sensitivity in half-life. Difficulties in the nuclear models used to calculate the matrix elements gives some uncertainty to the value of $\langle m_\nu \rangle$ derived for a particular $T^{0\nu\beta\beta}_{1/2}$.

It was recently shown [12] that the present data on oscillations leads very naturally to effective masses in the range $0.01\text{eV} < \langle m_\nu \rangle < 1\text{eV}$. In this report we show that this range of masses can be explored in the next several years with a large ^{136}Xe double beta decay experiment. The measurement of a non-zero $\langle m_\nu \rangle$, together with the oscillation data available, will then allow us to start the exploration of the CP phase in the lepton sector of the CKM matrix and will provide crucial input to cosmology.

2.4 Present status of $0\nu\beta\beta$ decay searches

Several experiments have been carried-on in the past searching for $0\nu\beta\beta$ decay and up-to-date no positive result has been reported.

Since the phase-space factor $G^{0\nu\beta\beta}$ is a steep function of the end-point energy ($G^{0\nu\beta\beta} \simeq (E_0^5/30 - 2E_0^2/3 + E_0 - 2/5)$ in the Primakoff-Rosen approximation), in practice only isotopes with the largest Q values can be used in a competitive fashion. In addition a likely candidate should have reasonable natural isotopic abundance. Finally, competitive experiments are generally performed in relatively deep underground sites where cosmic-ray background is reduced. In Table 1 we list the $\beta\beta$

decay candidates with $Q > 2$ MeV along with their isotopic abundance and phase space factors for $0\nu\beta\beta$ and $2\nu\beta\beta$ decays.

$\beta\beta$ decay candidate	Q (MeV)	Isot. Abund. (%)	$1/G^{2\nu\beta\beta}$ (yr)	$1/G^{0\nu\beta\beta}$ (yr)
^{48}Ca $\rightarrow^{48}$ Ti	4.271	0.187	2.52×10^{16}	4.10×10^{24}
^{76}Ge $\rightarrow^{76}$ Se	2.040	7.8	7.66×10^{18}	4.09×10^{25}
^{82}Se $\rightarrow^{82}$ Kr	2.995	9.2	2.30×10^{17}	9.27×10^{24}
^{96}Zr $\rightarrow^{96}$ Mo	3.350	2.8	5.19×10^{16}	4.46×10^{24}
^{100}Mo $\rightarrow^{100}$ Ru	3.034	9.6	1.06×10^{17}	5.70×10^{24}
^{110}Pd $\rightarrow^{110}$ Cd	2.013	11.8	2.51×10^{18}	1.86×10^{25}
^{116}Cd $\rightarrow^{116}$ Sn	2.802	7.5	1.25×10^{17}	5.28×10^{24}
^{124}Sn $\rightarrow^{124}$ Te	2.228	5.64	5.93×10^{17}	9.48×10^{24}
^{130}Te $\rightarrow^{130}$ Xe	2.533	34.5	2.08×10^{17}	5.89×10^{24}
^{136}Xe $\rightarrow^{136}$ Ba	2.479	8.9	2.07×10^{17}	5.52×10^{24}
^{150}Nd $\rightarrow^{150}$ Sm	3.367	5.6	9.35×10^{17}	7.84×10^{24}

Table 1: Double beta decay isotopes with $Q > 2$ MeV, from [11]. For ^{48}Ca and ^{96}Zr β decay is kinematically allowed but extremely suppressed by spin considerations.

In Table 2 we show the best sensitivity reached up-to-date for $0\nu\beta\beta$ decay. Although several experiments have been performed in which the $0\nu\beta\beta$ source is external to the detecting apparatus, there are clear advantages in schemes where the source is in a form that can serve also as detector for the electrons. Indeed the experiments showing the best sensitivity all utilize this principle.

$\beta\beta$ decay candidate	$T^{0\nu\beta\beta}_{1/2}$	Reference
^{48}Ca	$> 9.5 \times 10^{21}$ (76% CL)	[13]
^{76}Ge*	$> 1.1 \times 10^{25}$ (90% CL)	[14]
^{82}Se	$> 2.7 \times 10^{22}$ (68% CL)	[15]
^{100}Mo	$> 5.2 \times 10^{22}$ (68% CL)	[16]
^{116}Cd	$> 2.9 \times 10^{22}$ (90% CL)	[17]
^{130}Te*	$> 5.6 \times 10^{22}$ (90% CL)	[18]
^{136}Xe*	$> 4.4 \times 10^{23}$ (90% CL)	[19]
^{150}Nd	$> 1.2 \times 10^{21}$ (90% CL)	[20]

Table 2: Recent results in $0\nu\beta\beta$ decay experiments. Isotopes marked * are discussed in some detail in the text.

We concentrate here on ^{76}Ge, ^{130}Te, and ^{136}Xe that have provided the best sensitivity up-to-date.

$\beta\beta$ decay in ^{76}Ge had been studied using germanium diode ionization counters of very large volume. In this case the detector and the source are made of the same material and the event tagging is purely calorimetric. In recent times germanium detectors have been built out of isotopically enriched ^{76}Ge drastically improving the sensitivity. The isotopic separation and the clean condition used for a diode-quality crystal automatically provide low intrinsic detector background. The best sensitivity is achieved by the Heidelberg-Moscow experiment [14] at Gran Sasso, where detectors for a total of 11 kg (86% ^{76}Ge) have been taking data for 2.6 yrs. Typical energy resolutions of $FWHM \simeq 3$ keV at 2 MeV are achieved. This is the best figure obtained in any detector so far and it is particularly useful in discriminating between $0\nu\beta\beta$ (mono-energetic) and $2\nu\beta\beta$ (energy continuum). The total background observed in the detector is reported to be of 0.2 ev kg^{-1} yr^{-1} keV^{-1}. The half-life limit of 1.1×10^{25} yrs gives a neutrino mass limit of $\langle m_\nu \rangle < 0.46(1.3)$ eV using the "Quasi-Random Particle Approximation" or QRPA [21] ("Shell Model" or NSM [22]) for the nuclear matrix element calculation.

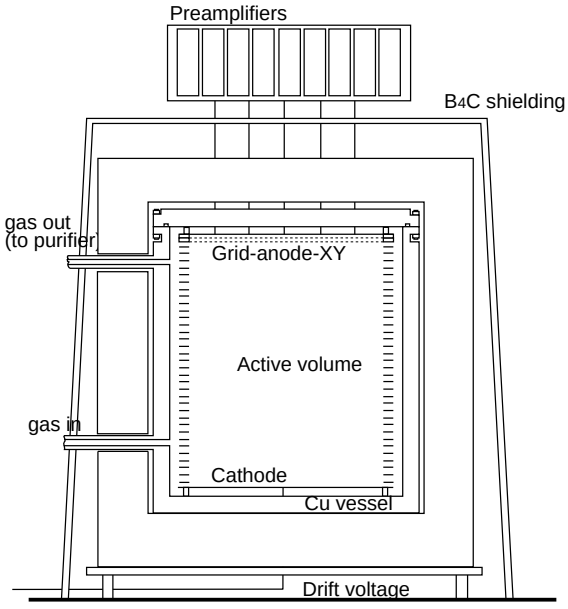

Figure 6: Scheme of the Gotthard TPC used in [19]. The total height of the active volume is 67.7 cm.

^{130}Te has the big advantage of a rather large isotopic fraction in natural tellurium (34.5%). However the realization of the particle detector is in this case more exotic. A calorimetric detector is possible by observing the temperature rise due to the electron energy being deposited in a TeO_2 crystal. This is only possible at very low temperature since the heat capacity is proportional to T^3 so that in cryogenic conditions a very small energy deposition causes a detectable temperature increase. In principle

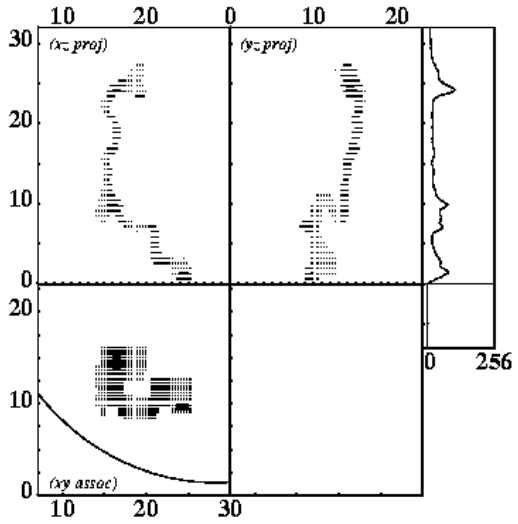

Figure 7: Electron tracks from a candidate double-beta decay event in xenon from [19]. The two main top panels show the xz and yz projections of the event, while the reconstructed xy view is given in the bottom part (dimensions are in cm). Pulse-height information is shown in the smaller panel on the right (in ADC counts). Note the higher ionization density at the end of the tracks. The circular sector in the bottom-left corner of the xy view represents the edge of the TPC.

the ultimate energy resolution of such detectors is superior to germanium diodes, although this has not yet been practically demonstrated in large crystals. The present limit [18] (Table 2) was obtained with a 334 g crystal of tellurium oxide running at a temperature of 10.5 mK. The detector has a resolution $FWHM = 16$ keV at 2.5 MeV and logged 171 days of data in the Gran Sasso Laboratory. The background reported in this case is 0.48 ev kg^{-1} yr^{-1} keV^{-1}. The resulting half-life limit of 5.6×10^{22} corresponds to a neutrino mass limit of $\langle m_\nu \rangle < 2.9(6.1)$ eV in the QRPA (NSM) approximation.

The search for $\beta\beta$ decay in ^{136}Xe needs substantially different techniques. Since Xe is a noble gas it is particularly advantageous to use the same gas as detecting medium in an ionization chamber. In modern times the "Time Projection Chamber" (TPC) configuration has been used, providing full spatial tracking of the electron trajectories with minimal extraneous materials in the active volume. The technique for background rejection is also quite different: while the energy resolution is not sufficient, alone, to completely suppress the background, the final event selection also uses the tracking information, showing the two-electron final state for the $\beta\beta$-decay case and only one electron from Compton scattering produced by most natural radioactivity backgrounds. The best sensitivity for ^{136}Xe has been achieved in a 5 atm TPC containing 5.3 kg of Xe enriched to 63% in ^{136}Xe operated inside the Gotthard road tunnel in Switzerland [19]. A sketch of this detector is shown in Figure 6.

The total running period was 1.47 yr and, although the energy resolution was $FWHM = 6.6\%$ at 1.592 MeV (105 keV), substantially worse than the figure obtained for germanium, the background was only 0.01 ev kg^{-1} yr^{-1} keV^{-1}[23], the lowest observed in any experiment. The superior tracking capability of this technique is apparent in Figure 7 where two projections ($x - z$ and $y - z$) for a double-beta decay candidate are shown. Since multiple scattering is substantial at 5 atm and no time-zero was provided in the Gotthard TPC, a two-electron event, like in the case of $\beta\beta$ decay, does not appear very different from a single-electron event produced, for instance, in a Compton scattering from background γs. In both cases multiple scattering of the low-energy track(s) is the dominant feature and two-electron events are selected only by observing the increase of specific ionization towards the end of the track(s). The number of such high ionization "blobs" effectively counts the electrons in the event. The resulting half-life limit of 4.4×10^{23} corresponds to a neutrino mass limit of $\langle m_\nu \rangle < 2.2(5.2)$ eV in the QRPA (NSM) approximation.

3 Detector design concepts

As described earlier $0\nu\beta\beta$ decay experiments represent the most sensitive means we have to directly measure neutrino masses in a region that is extremely important for particle physics and cosmology. The most sensitive searches for $0\nu\beta\beta$ to-date have used up to about 10 kg of nearly-pure isotopic species; hence further substantial progress can only be achieved through an ambitious program where *tons* of an appropriate isotope are monitored for a relatively long time. Indeed it is legitimate to ask whether backgrounds can be reduced to a small enough level such that full use can be made of the large mass of active material. This point is essential: in a background-free experiment the sensitivity to the half-life $T_{1/2}^{0\nu\beta\beta}$ is directly proportional to the number of nuclei N and exposure time t, so that the neutrino mass sensitivity scales as:

$$\langle m_\nu \rangle \propto 1/\sqrt{T_{1/2}^{0\nu\beta\beta}} \propto 1/\sqrt{Nt}. \tag{11}$$

However, unless some new technique is used, the small background observed in all the current experiments will increase with the mass and exposure time and become the true limiting factor of any kind of experiment. If we crudely assume that backgrounds increase linearly with Nt we would be in a regime where the sensitivity on $T_{1/2}^{0\nu\beta\beta}$ is limited by the statistical fluctuations in the background ($T_{1/2}^{0\nu\beta\beta} \propto \sqrt{Nt}/Nt$). Hence the neutrino mass sensitivity would scale only as:

$$\langle m_\nu \rangle \propto 1/\sqrt{T_{1/2}^{0\nu\beta\beta}} \propto 1/(Nt)^{1/4}. \tag{12}$$

Indeed this simple scaling only applies to backgrounds from materials that are internal to the active mass, since external backgrounds will be shielded to some degree from the larger mass. Still qualitative new means to suppress backgrounds are needed in order to fully utilize very large masses of $\beta\beta$ emitters.

^{136}Xe is an ideal isotope for this purpose since:

- it is one of the easiest isotopes to enrich;
- like argon, that is the mainstay of proportional chambers, it represents a good ionization detecting medium;
- most importantly its $\beta\beta$ decay produces a final state nucleus of ^{136}Ba that can be identified in its atomic form with powerful new techniques of high resolution optical spectroscopy.

Hence the classical technique of the Xe TPC, that has produced the smallest specific backgrounds reported up-to-date, will be supplemented with the system of ^{136}Ba identification, adding one new degree of freedom to be used for background reduction. The Ba tagging technique was first proposed in this context in[38]. While the size and properties of the TPC described here are very similar to chambers successfully

taking data since many years (see for instance [39]), the Ba tagging, that is new to particle physics, is a commonly used technique in atomic physics since many years.

Once the problem of reducing the backgrounds to negligible levels has been solved the only real challenge for this project is the procurement of ton quantities of ^{136}Xe . Since we expect the enrichment operation to last several years, this should be the first problem to be addressed in the quest for high sensitivity $\beta\beta$ decay experiments.

In the present chapter we will describe the detector system while in the next chapter we will discuss some of the issues related with the isotope separation. We will focus on the design of a modular detector that will initially need 1 ton of ^{136}Xe to operate. We will assume that while the first 1-ton module is commissioned, enrichment will continue and more 1-ton or 2-ton modules will be installed, up to a final active mass of 10 tons of ^{136}Xe . While it is premature to describe the exact detector parameters we will give here general design criteria and indicate the fields in which R&D is needed.

3.1 A large Xe gas TPC

The primary requirements for our TPC modules are:

1) Large size in order not only to have a few modules, but also to have the highest possible efficiency (fully contained events) and self shielding from backgrounds produced by external materials. Indeed the concept of TPC is ideal here because of the little extraneous materials present inside the detector;

2) Ability to withstand up to 10 atm pressure;

3) Good energy resolution in order to distinguish $0\nu\beta\beta$ from $2\nu\beta\beta$ decays;

4) Good spatial resolution in three dimensions (low diffusion and ability to provide the time when the event occurred (T0));

5) Low background environment;

6) Ability to neutralize Ba^{++} to Ba^{+} (or Ba^{0});

7) Ba^{+} (or Ba^{0}) lifetime in the chamber 10 s $< \tau_{Ba} <$ 1 hour, where the lower limit derives from the need to spectroscopically identify the Ba atom or ion and the upper limit insures that only a few Ba atoms or ions are present in the chamber at any given time;

8) Ability to perform laser spectroscopy within its entire volume.

While some of these requirements are in partial conflict with each other (for instance position resolution is best for small-sized chambers) we find a TPC containing about 1 ton of Xe a good tradeoff between all these requirements. One detector of

this size would be initially built, while the full mass of 10 tons will require adding more modules with similar features.

The use of liquid-xenon (LXe) in a TPC would result in a very compact detector with considerable economies. However the range of 1.2 MeV electrons in LXe is only 2.4 mm so that, given any conceivable spatial resolution, the topological information, and hence the main advantage of the TPC, would be lost. In addition, line broadening in LXe would be more important than in the gas, making the spectroscopic Ba-tagging more challenging.

Hence we concentrate here on a gas-phase TPC running at the highest possible density that still allows for a good topological signature. We fix our baseline design to a density of 30 g/l, corresponding to a pressure of ~ 5 atm at room temperature. This gives electron ranges of 21.6 cm at 1.2 MeV that are large enough to provide good spatial event reconstruction and background suppression, as shown by the successful operation of the Gotthard TPC. It is prudent, at this point, to maintain the option of a higher pressure (up to 10 atm) that could double the amount of ^{136}Xe in one chamber. The optimal pressure will be determined once the background rejection power of the laser tagging technique has been understood experimentally.

Our baseline design involves a chamber operated at room temperature. Some advantages may derive from operating the chamber immediately above the boiling point of xenon, since in this way the same density could be obtained at a lower pressure. In addition electron transverse diffusion in the TPC scales like $\sigma_x \propto \sqrt{T}$ so that at lower temperature somewhat better position resolution should be expected. Unfortunately the boiling point of xenon (165 K at 1 atm) is rather high with respect to lighter noble elements, so that in practice the density can be increased at most by a factor 1.5 and diffusion reduced by a factor $\simeq \sqrt{2}$. These gains may be offset, in part, by the fact that when running the chamber at room temperature radon and other radioactive contaminants can be removed more effectively by flowing the xenon through a cold trap. The extra complication and cost of operating a large chamber, with its high voltage system, in a cryogenic environment seem to disfavor this option for the time being.

The experiment will have to be located in an underground site in order to provide shielding against cosmic radiation. Since, as explained in the next Section, the size of a TPC module is quite modest the constraints of the underground laboratory are minimal and at present a number of sites in the US, Europe and Asia are under consideration. For this report we assume that the site chosen will have an overburden of at least $\simeq$ 2000 mwe (meter water equivalent) so that the cosmic ray muon flux is reduced to $< 10^{-2}\mathrm{m}^{-2}\mathrm{s}^{-1}$, corresponding to less than 0.1 Hz through the detector. Muons recorded in the TPC have a very distinctive signature and indeed were observed and easily rejected by the Gotthard group [23] based on track length, lack of scattering (high energy) and specific ionization. The last two features provide good discrimination even for tracks that clip a small corner of the chamber. The online trigger processor will be able to analyze and reject most muon tracks without acti-

vating the laser Ba-tagging system. Based on simple geometrical considerations we expect the laser beacon to be activated by muon tracks less than once per hour.

Some background will be caused by neutrons produced by muon spallation in the structures (rock and other materials) outside the detector. These fast neutrons enter the detector with some efficiency and produce spallation reactions on the xenon, carbon and hydrogen nuclei contained in the TPC. While the original muon and the neutron trail go undetected the spallation processes provide very distinct high ionization, short tracks that are very easy to distinguish and reject even at trigger level. We conclude that at the depth considered we do not need an active veto counter, as already found by the Gotthard group [23].

More serious is the background from natural radioactivity, either produced outside the TPC (mainly by the rock or concrete), or inside (mainly ^{222}Rn and, possibly, ^{85}Kr and ^{42}Ar). External backgrounds from the rock and concrete are attenuated by a $\sim$25 cm thick lead or steel enclosure and by the 1 cm thick pressure vessel that will be built out of low-activity steel. Additionally, cleaner shielding could be provided, if needed, by a layer of de-ionized water or mineral oil located inside the pressure vessel. While such layer could readily add a further factor of $\simeq$ 1000 of attenuation to 1.2 MeV γs (1 m of thickness), it would substantially complicate the design of the detector and make TPC repairs much more involved. Our preliminary estimates indicate that the external shielding alone should be sufficient for the experiment and, unless further background simulations will convince us otherwise, no liquid shielding should be implemented. In the following we conservatively assume that the TPC itself (without Ba-tagging system) will have the same specific rate of mis-identified background as the Gotthard experiment, and we rely on Ba-tagging for the final step of reduction. This hypothesis is conservative since the larger volume of our TPC provides better self shielding for the radiation produced externally. Internal backgrounds will be limited by careful choice of construction materials (essentially only copper, acrylic, Teflon and polyamide films) and by removing contaminants from the xenon as described in later Sections.

3.1.1 Chamber Layout

At 30 g/l (5 atm) 1 ton mass requires a volume of $\simeq$35 m^3. We design our chamber for 40 m^3 to allow for the addition of quenching gases as described in the next Section. As illustrated in Figure 8 the TPC volume will be defined by an acrylic cylinder of 3.2 m diameter and 5 m total length. The cylinder will also serve as rigid mechanical structure defining the position and distance of the different TPC components. A very thin cathode plane, formed by a copper coated Kapton membrane, will be placed half-way along the cylinder so that effectively the system will consist of two drift volumes and two anode readout planes, as customary in large TPC design (see for instance [24, 39]). At a drift field of 1 kV/cm each gap will require a total voltage of 250 kV that is still within the reach of commercial power supplies [25]. Field

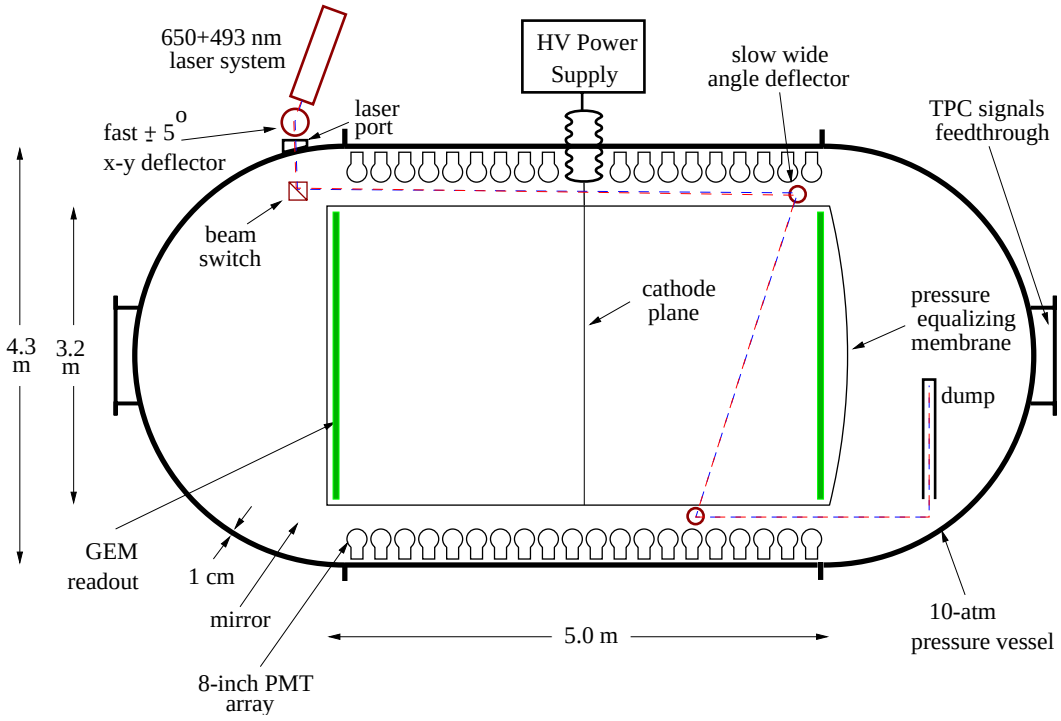

Figure 8: Conceptual layout of the detector. The TPC is surrounded by a layer of gas that electrically insulates it from and transfers the pressure to the external pressure vessel. The HV feedthrough will require the omission of a few photomultipliers. Another independent laser system will probably be needed to illuminate the left half of the chamber. Such system will probably be set on a different plane and be essentially the mirror image of the one indicated. A rather elaborate system of windows, baffles and mirrors will be needed in order to feed and remove the laser beam from the chamber without causing undue scattering of light into the photomultipliers. All laser beam handling parts will be located away from the cathode plane that is biased at about -250 kV respect to ground. Not shown in the drawing is the external γ-ray shielding. Materials used for the construction of the chamber itself will be intrinsically clean, like acrylic, Teflon, Kapton and copper, while the pressure vessel will be built out of carbon steel. Low activity glass will be used for the photomultiplier tubes.

shaping electrodes will be installed on the inner surface of the acrylic cylinder either by mounting solid copper rings or by depositing copper strips. The resistive chain will be located outside the cylinder. Given the size of the end-plates we do not favor at this time the use of wires for the signal amplification and readout, rather we plan to use Gas Electron Amplifier plates ("GEM") [26] as described in more detail in a later Section. The 5-10 atm pressure will be contained by a metallic vessel isolated from the cathode plane by pressurized gas. The acrylic cylinder will be closed at one end by a solid acrylic plate and at the other by a flexible membrane (or bellows) made out of a thin plastic film like mylar or nylon. Such membrane will confine the xenon to the TPC active volume while absorbing small pressure differences between the xenon and the buffer gas. An inert gas also pressurized at 5 atm will fill the volume between the pressure vessel and the TPC proper. 8-inch diameter photomultipliers will be installed on the inner surface of the pressure vessel, in order to detect photons from Ba^+ fluorescence and from Xe scintillation. It is easy to find standard 8 inch tubes that are able to safely operate at a pressure of 5 atm. Larger pressures may require a special glass envelope. Studies will be performed to ascertain what level of glass impurities will give tolerable backgrounds. Assuming the inert gas to be nitrogen we would need 20 cm between the central cathode edge and the closest photomultiplier in order to hold (at 5 atm) the 250 kV. The use of heavier gases (like Kr or CBr_4) that would also provide some shielding is currently under consideration. Since the photocathodes are located at a radius of 1.8 m, full photomultiplier coverage of the cylindrical surface with a square lattice would require about 1300 photomultipliers and give a photocathode coverage of $\simeq 60\%$ (there is no coverage at the two chamber ends where the anode planes are located). While much smaller coverages (down to $\sim 10\%$) would be acceptable for the barium spectroscopy, relatively large acceptance is needed in order to effectively use the scintillation light to complement the energy measurement. The possibility of reducing the number of photomultipliers and re-direct the light with mirrors and wavelength shifters looks rather promising but further work is needed in order to ascertain whether the smearing in the timing poses any problems.

Since photomultipliers with base need 35 cm of longitudinal clearance, the inner surface of the pressure vessel has to have a radius $r = 215$ cm. In order to withstand a pressure of up to $P = 10$ atm the vessel has to have a thickness of $t = Pr/2\sigma$ where σ is the strength of the material. We use $\sigma = 1300$ atm (having applied a safety factor of 2 to the figure for carbon steel) and obtain a thickness of 1 cm, that is rather common for large vessels. Appropriate reinforcements will have to be applied at the flanges, where the hemispherical bulkheads are mounted and around the points where the cylinder rests on a saddle. A special system with double o-rings and the middle volume purged by a vacuum pump will be used in order to exclude the possibility that leaks could result in loss of xenon.

We anticipate mounting the laser systems (at least two, one for each half chamber) outside the pressure vessel for easy maintenance, while the beam steering systems will

be located in the hemispherical bulkheads. The entire laser transport and steering system will have to be engineered so that the beam(s) will enter the chamber and exit to a dump through a low-loss system. This will be essential to minimize the light scattering onto the photomultipliers. While the details remain to be decided, it is likely that a rather large number of entrance and exit windows (not shown in Figure 8) will be required.

Along with the above baseline design we are considering the possibility of using the acrylic cylinder itself as pressure vessel. Since σ for acrylic is about 5 times smaller than for steel but the radius of the vessel would only be 160 cm, the thickness in this case would be 4 cm. Substantially larger acrylic structures, like the SNO D_2O containment sphere, have been built. The hemispherical bulkheads would be made out of steel since no optical access is needed at those locations and the electrodes near the anodes are close to ground potential. Steel traction rods would be used to secure the bulkheads against the o-ring seals. While acrylic has been successfully used in large TPCs [27] some material tests will be required to insure that outgassing at room temperature will not excessively reduce the electron lifetimes in the chamber.

3.1.2 Gas System

The choice of a gas mixture for the TPC is essential for the good performance of the experiment. A secondary gas, mixed in small quantities with the xenon, has to:

- quench the xenon UV scintillation so that a gain of a few hundred can be obtained in the gas under stable conditions;
- re-emit the UV light in some detectable form so that its energy and timing information can be recovered and used;
- provide high electron drift velocity in order to reduce electron diffusion and improve the TPC position resolution;
- be available in high enough purity to allow for long electron lifetimes and low activity;
- neutralize Ba^{++} to Ba^{+} while providing a stable environment for Ba^{+} ions;

In the following we will discuss some of these items in detail. In Table 3 we list the ionization and excitation properties for some common hydrocarbons along with Xe and Ba.

It is known [28] that it is quite difficult to obtain electron multiplication and stable operation in xenon chambers. This is due to the far UV scintillation light ($\lambda_{\rm scint} \simeq 178$ nm corresponding to 6.93 eV) copiously produced with the multiplication process that in turn ionizes the gas and extracts electrons from the metallic surfaces. The addition of a quencher gas that absorbs the UV radiation usually restores the proportionality and stability of the chamber. In our case this particular requirement

is greatly relaxed by the use of GEM planes instead of a more conventional anode wire array for the chamber readout, since the confined GEM geometry (as opposed to the open wire geometry) drastically limits the solid angle available to the UV radiation. Indeed the operation of GEMs with high gain in pure xenon has been reported in the literature [29]. Despite this, it is still desirable to absorb the UV scintillation light and convert it into more convenient forms of excitation, so that better energy resolution and timing information can be obtained. In fact it has been shown [31] that, at least in LXe, not only the energy from the scintillation is a substantial fraction of the total energy deposited, but the two fractions are anticorrelated, so that the coherent sum of both energies, if appropriately weighted, can substantially decrease the fluctuations present in each of them. Two techniques can be used to recover the energy information associated with the xenon scintillation:

a) a wavelength shifter gas can be added to the xenon in order to re-emit the light in the blue or green, where the quantum efficiency of conventional photocathodes is maximum and there is no risk of secondary ionization in the chamber;

b) a film of material with large photoionization cross section (like for instance CsI) can be deposited on the surface of the GEM facing the drift volume. As shown in [30] the secondary electrons produced when the UV scintillation radiation strikes the GEM are effectively collected in the channels and multiplied, providing a fast $T0$ signal.

a) requires a gas with ionization potential $IP > 6.93$ eV and has the advantage of automatically providing a fast light signal to be used as $T0$. However a large photocathode coverage is needed in order to be able to fully collect the energy from scintillation. b) has the advantage of simplicity as the collection of all of the energy is done at the anode in the ionization channel. However the solid angle for collection is limited by the size of the GEM plane and in our case some photomultiplier coverage is needed anyway in order to perform the Ba^+ tagging. Furthermore it might be difficult to obtain CsI low enough in radioactivity for the experiment. Hence at present time we favor a) that can be implemented with several of the molecules listed in Table 3. However tests will have to be performed in order to measure the scintillation recovery efficiency of each molecule. The drift velocity that one can attain for each of the two options will also be investigated in some detail.

Before discussing the conversion of Ba^{++} into either Ba^+ or Ba in a buffer gas we explore here the possibility that the Ba^{++} ion would be neutralized to either Ba^+ or Ba by the trail of electrons produced by the βs in the double-beta decay. We can easily estimate the magnitude of this effect. Each β has an energy of $\simeq 1.2$ MeV and, at 5 atm of pressure, ranges out in 21 cm. The maximum specific ionization (~ 1 MeV/cm) occurs at the end of the track, too far from the Ba^{++} to have any effect. At the beginning of the β track the specific ionization is $\simeq 3 \times 10^{-2}$ MeV/cm, corresponding to a trail of $\simeq 2500$ electrons/cm or, on average, one electron every

Common name	Formula	Ionization Potential (eV)	Fluor. Peak (nm)	Molar Extinction ($mol^{-1}cm^{-1}$)	Q.E.	Vapor Press. at 300 K (atm)
Nitric Oxide	NO	9.26				gas
Methane	CH_4	12.51			0.0	gas
Acetylene	C_2H_2	11.40			0.0	gas
Ethylene	C_2H_4	10.51			0.20	gas
Ethane	C_2H_6	11.52			0.0	gas
Methylal	$C_3H_8O_2$	9.7				
Allene	C_3H_4	9.53			0.55	
Propane	C_3H_8	10.95				9.85
Butane	C_4H_{10}	10.53				2.55
1-Butene	C_4H_8	9.45			0.21	2.92
Isobutane	C_4H_{10}	10.57			0.0	3.65
Propene	C_3H_6	10.57			0.22	
Isobutene	C_4H_8	9.24			0.20	2.96
Cyclohexene	C_6H_{10}	8.95			0.10	0.116
Cyclohexane	C_6H_{12}	9.86			0.10	0.128
Benzene	C_6H_6	9.25	277	200	0.07	0.104
Toluene	C_7H_8	8.82	284	280	0.17	0.0374
m-Xylene	C_8H_{10}	8.56	290	720	0.17	0.0108
bis-MSB	$C_{24}H_{22}$		420	54000	0.94	
1,1,4,4,Tetraphenyl-butadiene	$C_{28}H_{22}$		450	36000	0.60	
PPO	$C_{15}H_{11}NO$		360	32000	1.00	
Naphtalene	$C_{10}H_8$	8.14	330	5500	0.23	1.08×10^{-4}
Azulene	$C_{10}H_8$	7.42	375	4800	0.03	9.87×10^{-6}
Anthracene	$C_{14}H_{12}$	7.55	$\sim$ 400	10000	0.36	
Acridine	$C_{13}H_{11}$ N		420	12000		
Aniline	C_6NH_7	7.72	320	1700	0.08	8.88×10^{-4}
Trimethylamine (TMA)	$(CH_3)_3N$	7.82			0.23	
Triethylamine (TEA)	$(C_2H_5)_3N$	7.50			0.15	0.072
Tetramethyl-germanium (TMG)	$(CH_3)_4Ge$				0.50	
Tetramethyl-silane (TMS)	$(CH_3)_4Si$				0.20	
Tetrakis(dimethylamine)-ethylene (TMAE)		5.4				6.6×10^{-9}
	Xe	12.127	178 nm (scint.)	-	-	-
	Ba	5.210	see text	-	-	-
	Ba^+	10.001	see text	-	-	-

Table 3: Useful properties for a few common substances. Fluorescence properties are taken from [32, 33] while all other data is derived from [34, 33]. Ionization potentials for Xe and Ba (in the neutral and first ionization state) and Xe scintillation wavelength are also listed for convenience. The "Molar Extinction" coefficient is defined as the attenuation length of a mole of material for light in the absorption band. Q.E. refers to the quantum efficiency for photon re-emission in the substance. Empty spaces are left whenever the corresponding parameter is not know to the authors, a dash (-) indicates that the corresponding parameter does not apply to the substance.

4 μm. The electrostatic field on the electrons due to the Ba^{++} ion is then about 10 V/4 μm or 2.5 kV/m, substantially smaller than the electric field from the TPC ($\sim$ 100 kV/m) that will tend to sweep the electrons away from the positive ions. Our conclusion is that the fraction of ions neutralized by the ionization trail is negligible

and therefore the conversion of the Ba^{++} into either Ba^{+} or Ba has to be accomplished by charge exchange collisions with trace organic molecules either in the quencher gas itself or in another gas added for this purpose. Collisions with Xe will not change the ionization state of the barium since the ionization potential (IP) of Xe is 12.127 eV, greater than that of Ba^{+} (10.001 eV) or Ba (5.2 eV). As shown in Table 3 linear-chain hydrocarbons that are commonly used to quench discharges and reduce diffusion in ionization chambers tend to have IPs above 10 eV, too high for our purpose of charge exchange with Ba^{++}. However most cyclic or aromatic hydrocarbons have IPs between 8 and 10 eV, ideally placed to neutralize Ba^{++} to Ba^{+}, yet maintaining Ba^{+} as a stable ion in the chamber. While a-priori we do not anticipate any problems with this technique, some tests with a small TPC will be performed to establish the suitability of some of the hydrocarbons with $IP < 10$ eV as quencher in the chamber. A second preliminary experiment will be necessary to study the charge exchange processes for Ba^{++} and Ba^{+} and ascertain the relative merits of the different possible gas mixtures. This could take the form of an ion trap experiment in which gases are added to a cloud of Ba^{++} and Ba^{+} initially in high vacuum, or an experiment in which an atomic or ionic beam is studied in a gas cell.

Finally we expect to recirculate continuously the gas mixture from the chamber in order to remove radioactive isotopes and "electron-hungry" molecules that attach to the drifting electrons and attenuate the electron yield from large distances. This second task is usually achieved with Oxysorb cartridges [35] and purities of 10 ppb in gaseous argon have been achieved. Radioactivity filtering has to address primarily radon that is continuously produced by the decay-chain of uranium contained in small amounts in the materials used to build the detector. Radon is most effectively removed using cold traps where it freezes at a temperature that is substantially higher than the boiling point of xenon.

3.1.3 Readout System

As mentioned above our chamber is probably too large to use wires for signal amplification and collection. Long-wire instabilities, along with abundant UV production at the wire plane would make stable operation quite challenging. We are planning to obviate this problem by using Gas Electron Multipliers (GEMs) [26]. GEMs have been already considered as readout systems for TPCs [36]. As shown in Figure 9 in this scheme the anode wire arrays of the chamber would be replaced with a thin Kapton foil, metallized with copper on both surfaces. Typical Kapton thickness is 50 μm with few μm copper cladding. Small holes are etched into the foil with an appropriate tapered profile using a lithographic process. Typical hole sizes vary between 40 and 140 μm while hole pitches between 90 and 200 μm have been used. The upper copper layer defines the end of the TPC drift cage while the bottom layer is biased at a more positive potential (a typical gap voltage is 500 V). As a result, while the TPC drift field remains very uniform down to a distance from the GEM of the

order of the hole-size, the electrons are "funneled" into the holes with high efficiency and inside the holes experience a very high electric field that leads to avalanche amplification. The amplified signal can then be picked up in several modes. As shown

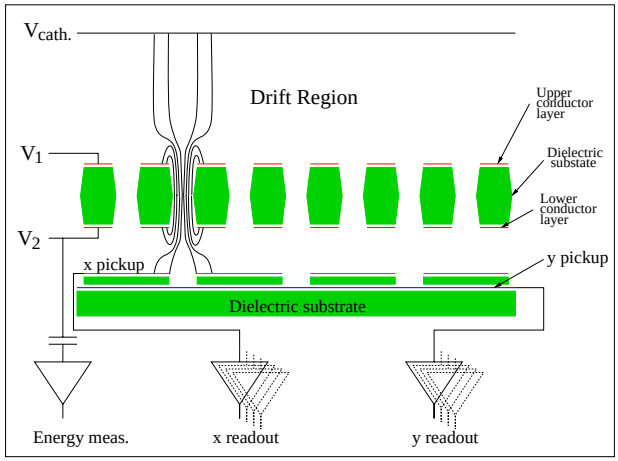

Figure 9: General layout of a Gas Electron Multiplier (GEM) as readout element of a TPC. The TPC drift volume it on the top part of the figure. V_{cath} is the TPC cathode voltage (typically -250 kV in out case), V_2 is biased close to ground potential while V_2 is kept more negative in order to establish a large-enough field to obtain electron multiplication in the holes. The good mechanical tolerances needed on the size and shape of cladding and substrate holes can be achieved with a lithographic process. While the total energy is measured by reading-out the charge on the bottom GEM electrode, x and y information is provided by orthogonal strips also obtained with by lithography on a kapton substrate.

in Figure 9 a convenient scheme for our application could consists in building, again with microlythographic techniques, two arrays of x and y strips to be located below the GEM. While such array would provide the spatial readout of the chamber, the total energy, that needs to be known with good resolution, can be obtained by reading out the bottom surface of the GEM itself (with appropriate DC decoupling). We anticipate feeding the energy signal to a very low noise amplifier and precision digitizer chain, while the information from the position readout strips will be fed to a system of flash ADCs. A readout pitch of 2 mm would require 3200 electronics channels on each end of the TPC while a very reasonable sampling rate of 10 MHz would provide sufficient z resolution. Relatively inexpensive flash ADCs with these properties have been designed for the ICARUS experiment [37] and are now commercially available. In parallel with this system an array of discriminators will provide more limited information to a trigger processor that will be able to flag events for recording and, more important, point and fire the laser system as described below.

3.2 Barium spectroscopy and atom tagging

As described above, extrapolating the radioactive backgrounds observed in any of the present generation $\beta\beta$ detectors, much larger experiment are predicted to be background dominated. Indeed large volumes provide additional self-shielding and small improvements can be obtained by careful workers, however it is clear that only qualitatively new tools can provide the improvement of performance needed for a substantial and worthwhile new effort in the search for $0\nu\beta\beta$ decay. The use, for the first time, of highly selective laser detection of the final atomic state, would provide an entirely new process for the rejection of radioactive backgrounds.

Single atom laser detection methods are new to particle physics but have become widely used in atomic physics in the last twenty years, and were recognized in the 1990 Nobel Prize award [40] to Dehmelt, Paul, and Ramsey. Resonant laser detection is both highly sensitive, yielding $\geq 10^7$ photons per second from a single atom, and highly selective, since this large scattering rate only occurs over a narrow band of frequencies which are unique to each element. Moreover, the atomic physics community has had twenty years experience in observing single barium atoms, since it was the first atom to be observed [41] in 1978 and in some ways it is the easiest atom to detect.

In the following we will review the history of recent atomic physics work on single barium atoms, consider the effect of high pressure xenon on the laser detection process and outline the laser apparatus required to observe resonant scattering in a large-volume, high-pressure TPC.

3.2.1 Laser Detection of Single Atoms in Atomic Physics

Single atom laser detection techniques have become widely used in atomic physics in the last few years. Single barium ions were first observed in 1978 by Dehmelt [41] and collaborators using a radio frequency quadrupole trap and laser cooling. These traps use electromagnetic forces to suspend the ion in ultra-high vacuum while a laser is used to cool the ion to temperatures of a few millikelvin. Laser cooling is nowadays common in atomic physics and was recognized in the 1997 Nobel prize award to Chu, Cohen-Tannoudji and Phillips. The cold ion is confined to a region a few nanometers from the center of the trap where it is free from Doppler broadening and collision effects so that it behaves like an ideal single atom previously considered only in gedanken-experiments. The study of single trapped atoms has provided order-of-magnitude improvements in frequency standards as well as qualitatively new work in quantum optics, quantum computation, chaos, and Wigner crystallization. At present three groups are operating ion traps using Ba^+, while about a dozen others are studying single trapped ions of other elements, including calcium, strontium, magnesium, and beryllium.

The level structure of the $^{136}Ba^+$ ion is shown in Figure 10. It is typical of an alkali atom which has single valence electron outside a closed shell. There is a strong

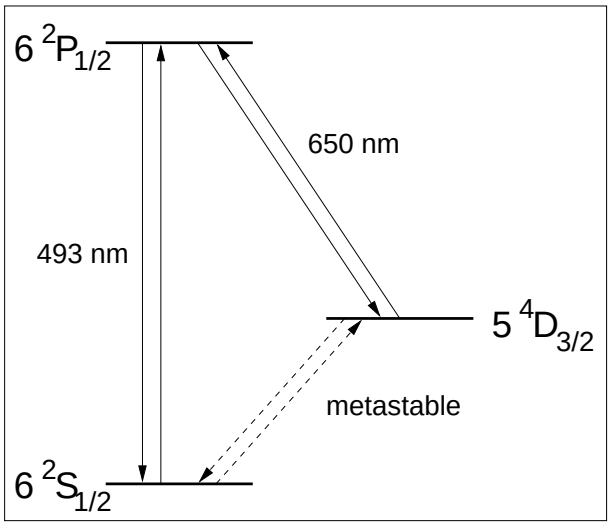

Figure 10: Atomic level scheme for Ba^+ ions.

allowed transition at 493 nm between the $6^2S_{1/2}$ ground state and the first excited state $6^2P_{1/2}$ and a weaker transition between the $6^2P_{1/2}$ and the meta-stable $5^4D_{3/2}$ separated by 650 nm. The 493 nm transition has a spontaneous lifetime of 8 ns and when saturated will radiate 6×10^7 photons/s. The branching ratio of decay into the D (S) state is 30% (70%).

3.2.2 Barium Detection in High Pressure Xenon

The primary difference between the single atom work done previously and this experiment is that here the Ba^+ ion is observed in a buffer gas of several atmospheres of xenon. This is in contrast with the ion trap work which limits the buffer gas pressures to 10^{-8} atmospheres. The high pressure xenon has two effects: first, it obviates the need for a trap since diffusion in the dense gas is sufficient to confine the atoms for long enough time to obtain a signal; second, it pressure broadens the optical transitions which increases the laser power required.

Diffusion can be understood as a random walk problem. The mean free path ℓ in Xenon at 5 atm is 2 nm and the mean time between collisions is $\tau = 8$ ps. The total distance L traveled in a time t will then be $L = \ell\sqrt{n}$ where $n = t/\tau$. Therefore the barium ion will diffuse only $\simeq 0.7$ mm in 1 s and during this time it will scatter $\geq 10^7$ photons.

Pressure broadening can be understood as a simple application of the Fourier Theorem. The mean time between collisions at 5 atm of 8 ps is 1000 times shorter than the 8 ns spontaneous emission lifetime. Each collision randomizes the phase of the atomic dipole, and therefore reduces the time over which the optical frequency

is defined. The pressure broadened line-width is therefore 1000 times greater than the natural line-width of 20 MHz. The pressure of 5 atmospheres corresponds to a 20 GHz full-width-half-maximum (FWHM) Lorentzian line-shape function.

The most significant effect of pressure broadening is that it increases the laser power required to achieve the maximum photon scattering rate of 6×10^7 photons/s, called the "saturation" laser intensity $I_{\rm sat}$. The pressure broadened line-width is thus a key experimental parameter since it sets the overall laser power and thus defines the type of laser technology required. For most atomic systems, $I_{\rm sat}$ is proportional to the pressure, so that 5 atmospheres of Xe will require a laser intensity of ~ 5 W/cm^2. For each event the TPC will conservatively provide a region of interest of 3×3 cm^2 so that the laser power needed would be ~ 50 W. CW lasers of this power level are not available commercially, so that one must either operate below saturation where the scattering rate is $\propto I/I_{\rm sat}$, or use a more tightly focussed scanning beam, or use pulsed lasers. One should note that although previous single atom experiments have operated in the saturated regime, they have also used small solid angles ($\approx 10^{-3}$) for the photon detection. The much larger solid angle coverage (≈ 0.1) contemplated here can therefore compensate for the lower photon emission rate expected in a non-saturated regime. If saturated operation is desired a synchronously-pumped mode-locked pulsed laser can be used which generates a train of high power picosecond pulses with a repetition rate of $\approx$ 100 MHz. Because of the 8 ns lifetime of the Ba^+ fluorescence, the 100 MHz repetition rate will lead to quasi-CW photon emission which will approximate the maximum saturated value. Because the value of $I_{\rm sat}$ determines the overall design of the detection system, it is important to measure the pressure-broadening parameters of Ba^+ in a small-scale preliminary experiment. In the density-matrix theory of laser-atom interactions, this comprises a measurement of relaxation times for the diagonal and off-diagonal density matrix elements, called T_1 and T_2 respectively, which completely determine the response of the atom to laser light.

Apart from these effects one may worry that the physical size of the chamber in which we want to detect single atoms is very large and some direct light from the laser may scatter on small particles and impinge on the photomultipliers, simulating the barium detection. Three additional methods that can be used to make the detection un-ambiguous.

- The first method uses the meta-stable D state as a bottleneck in an optical pumping cycle. The result is that the blue 493 nm light can be switched on and off by modulating the 650 nm red light. This gives an unmistakable signature that the light comes from the specific atomic species sought. The applicability of this method depends on the effect of the xenon buffer gas on the D-state lifetime, which is not known at present and will be investigated experimentally.

- The second method uses an electro-optic frequency modulator to shift the frequency of the 493 nm laser light without changing its intensity. Current devices

can shift the frequency by 20 GHz in about 500 ns. Modulating the laser frequency in this fashion, the presence of the right atomic species would then be signaled by a modulated count rate, which would distinguish it from simple scattered light.

- The third method can be used in conjunction with pulsed laser excitation, and utilizes the 8 ns spontaneous emission lifetime of the barium atoms to discriminate between resonant laser excitation and scattered background light. The scattered light will have time-dependence of the picosecond excitation pulse, while emission from Ba^+ will decay exponentially with an 8 ns lifetime. A histogram of the photon arrival time will therefore provide another discriminant for the detection of Ba^+.

The use of one of the above methods or a combination of them together with careful masking should make the atom detection, even for a very large volume, very reliable.

3.2.3 Laser Detection System

The laser detection system consists of three major parts: the laser source, the beam pointing system, and the photomultiplier detection array.

Double beta decay of ^{136}Xe produces the doubly ionized isotope $^{136}Ba^{++}$, which cannot be detected using current laser technology since its transitions lie below 150 nm, where efficient laser sources do not exist. However both the singly charged ion Ba^+ and the neutral atom Ba are suitable candidates for laser detection. Ba^+ has a strong dipole allowed transition from the 6S to the 6P state at 493 nm while neutral Ba has a similar transition at 554 nm. Both transitions lie in the visible part of the spectrum where powerful lasers and detectors with high quantum efficiency are available. We will discuss the case of Ba^+ in the following.

The trigger for the laser system is provided by the TPC detecting two electron-type events. It takes several hundred microseconds for the ionization trails produced by the electrons to drift to the TPC gain region and collection pads or wires. The signals amplified by the front-end electronics are then fed to a trigger processor that produces an estimate of the location of the potential double beta decay candidate. Based on our experience with complex pattern recognition trigger processors [42] we expect to be able to provide a trigger in much less than 10 ms. A beam pointing system can utilize two classes of devices: galvanometer driven mirrors, which have millisecond response time and can swing by any angles, and acousto-optic beam deflectors, which have microsecond response time but more modest (few-degrees) deflections. As shown in Figure 8 we anticipate using a set of galvanometer driven mirrors to point the laser to the appropriate spot in the chamber, while a pair of acousto-optic deflectors could be used to perform a "raster scan" locally and pinpoint the exact location of the Ba^+-ion. The same array of photomultipliers discussed in the context of the xenon scintillation

light detection will then be used to detect the Ba^+ de-excitation photons that are in the blue close to the maximum quantum efficiency for bialkali photocathodes.

Resonant excitation of the Ba^+ ions will produce $> 10^7$ photons per second, which is sufficient to identify the atom in a fraction of a second. Assuming very conservatively that the photomultipliers cover a solid angle of 10% and that they have a quantum efficiency of 10%, the detected resonant count rate will be >100 kHz. Thus a 1 ms integration time will yield 100 counts, which will be distributed among a large number of different photomultipliers. An appropriate majority logic can suppress accidental dark counts from each photomultiplier while yielding a positive coincidence signal. As discussed, non-resonant scattered light from the laser beams can be suppressed by a lock-in scheme which either frequency-modulates the lasers off the atomic resonance or intermodulates the fluorescence using an optical pumping bottleneck, as described. We expect to be able to reduce the background from scattered light to negligible levels. We note that an atom observation period of 1 s is extremely conservative: as discussed above the barium ion will diffuse $< 1\mu$m in 1 ms, so if needed it is easy to imagine extending the observation period to several seconds in order to enhance the signal-to-noise ratio.

The detailed design of the laser system depends on the results of the preliminary experiments to study pressure broadening and charge exchange, as discussed above. The charge exchange experiment will determine whether to use Ba^+ or Ba for the laser detection. While both cases are feasible, in the case of Ba^+ the laser technology involved is simpler. The pressure broadening experiment will determine the required laser power, which in turn will influence the choice of CW or pulsed laser excitation. Since the experiment must operate with minimal attendance for many months, a solid state laser system is preferred. With present technology the most reliable system would be a frequency-doubled laser diode, such devices are non-critical and commercially available at 986 nm for doubling to 493 nm for Ba^+.

3.2.4 Possible Applications of Atom Tagging at High Pressures

The ability to reliably detect one impurity atom in 10^{25} background atoms may have an impact on the technology of ultra-pure materials, which underlies the semiconductor industry. Our detector will be many orders of magnitude more sensitive to barium impurities than any previous device and will be sensitive to phenomena at vapor pressures of $\approx 10^{-20}$ torr that have never before been observed.

3.3 Estimated Detector Performance

The combined use of topology and energy information from the TPC and Ba^+ identification from the laser system will provide a very robust experiment and allow us to fully exploit the unprecedented mass of an isotopic species that we are considering. Indeed the project described here represents a large qualitative new step in the

exploration of double-beta decay and one of the best hopes we have to discover and measure a non-zero neutrino mass in the near future.

We can crudely estimate the position and energy resolutions for our chamber from an extrapolation using the Gotthard TPC. Assuming a drift velocity similar to the one in Gotthard and a drift distance of 250 cm (3.6 times larger than the Gotthard case) we obtain transverse and longitudinal position resolutions (σ) of better 5 mm. This figure should give us roughly the same background suppression factor as obtained at Gotthard, since the important parameter here is the ability to identify the "blobs" of increased specific ionization for tracks that have a range of 21 cm. Furthermore the ability to measure $T0$ will enable us to longitudinally locate each event, so that possible external backgrounds from the anode and cathode planes can be better understood.

Energy resolution should be no worse than the $\sigma_E/E = 2.8\%$ (at 1.592 MeV) obtained at Gotthard, since in addition to the total charge, also the scintillation light will be collected[31].

In addition the possibility of using the laser tagging system with a small spot-size in a "raster scan" mode around the event location, will enable us to measure with mm resolution the position of the decay and hence the point along the tracks where the two electrons were produced. Hence one would be able to perform a constrained kinematical fit to the event where amount of ionization and scintillation, number of "blobs", electrons angular correlation and range for *each* of the electrons would all be taken into account. In the following we will use a very conservative energy resolution of 2.8% for the first phase of the experiment (5 ton yr), while a more aggressive 2% will be used for the ultimate (100 ton yr) case.

While the quantitative advantage of each of the techniques discussed will be better understood after extensive laboratory tests and a full Monte Carlo simulation, here we simply assume that the above methods, together with the Ba^+ identification, will reduce the sum of all radioactivity backgrounds by at least three orders of magnitude with respect to the Gotthard case, making a 10-ton ^{136}Xe experiment essentially background free. From the size and geometry of the chamber we obtain an efficiency for fully contained events of 70%. In Table 4 we compare the projected sensitivity of this experiment with the present limits on $0\nu\beta\beta$ decay.

It is interesting to note that for these very large quantities of material the background on $0\nu\beta\beta$ decay from the well known $2\nu\beta\beta$ mode becomes important. As already remarked this "background" is obviously not suppressed by the laser tagging methods, and, since its only distinctive feature is the electron energy spectrum (see Figure 5), kinematical reconstruction is the only effective tool.

Before discussing this last step of data reduction we briefly discuss the $2\nu\beta\beta$ sample that this project would produce. Assuming that the $2\nu\beta\beta$ half-life is 8.5×10^{20} yr [43] we will already have 8.6×10^6 decays (at 70% reconstruction efficiency) after the first phase of the experiment (5 yr ton). This number of events can be compared to the ~20,000 $2\nu\beta\beta$ events observed in ^{76}Ge [44], and ~1500 events in ^{100}Mo and

Isotope and Reference	Total Mass (kg)	Enrich. grade (%)	Det. eff. (%)	Meas. time (yr)	Bkgd. ($kg^{-1}yr^{-1}$ keV^{-1})	$T_{1/2}^{0\nu\beta\beta}$ (yr)	$\langle m_\nu \rangle$ (eV) QRPA	NSM
^{76}Ge [14]	11	86	100	2.6	0.2	1.1×10^{25}	0.46	1.3
^{136}Xe [19]	5.3	63	30	1.47	0.02	4.4×10^{23}	2.2	5.2
^{130}Te [18]	0.33	34.5	100	0.45		5.6×10^{22}	2.9	6.1
^{136}Xe this proj.	1000	65	70	5	0^*+ 1.8 events	8.3×10^{26}	5.1×10^{-2}	0.14
^{136}Xe this proj.	10000	65	70	10	0^*+ 5.5 events	1.3×10^{28}	1.3×10^{-2}	3.7×10^{-2}

Table 4: Comparison between the parameters and results achieved by the best present double-beta decay experiments and the project described here. As explained in the text the new techniques that we plan to use to reduce the background are essential to fully utilize the large mass of isotopic species. All other experimental parameters are assumed to be the same as in the Gotthard experiment. We list here, together, the case of an initial detector with 1 ton of xenon and the final results possible with 10 tons of xenon and a very long (10 years) data-taking period. The ^{136}Xe enrichment grade used here is intermediate among the options (and price ranges) shown in Table 5. The quantities marked with * are radioactivity backgrounds that are assumed to be negligible as discussed in the text. In addition the background from mis-identified $2\nu\beta\beta$ decays is also shown in total events in each exposure.

^{116}Cd [45]. The project described here will increase, as a "by-product", the world sample of $2\nu\beta\beta$ decay events by about three orders of magnitude. The combination of TPC and laser tagging will enable full kinematic reconstruction of the events (as it was done in [45] for the ^{100}Mo and ^{116}Cd cases), so that we will be able to measure not only the sum energy spectrum, but also determine the vertex position, and therefore observe the single electron spectra and the two-electron angular correlations. This will enable us to study in detail the mechanism of the $2\nu\beta\beta$ decay and check for deviations from the pure Gamow-Teller decay, checking, for example, effects of weak magnetism-induced terms.

Moreover, with this unprecedented statistics of events reconstructed with high quality one will be able to search for the neutrinoless decay with Majoron emission, which, as shown in Figure 5, would manifest itself as a small deformation of the $2\nu\beta\beta$ continuum spectrum.

While the $2\nu\beta\beta$ mode is interesting on its own right, a reasonable resolution on the total energy measurement will remove it effectively and hence obtain a background-free sample for the $0\nu\beta\beta$ mode. We select events in the interval $I_+ = [Q_{\beta\beta}, Q_{\beta\beta} + 2\sigma_E]$ (where, as discussed, $\sigma_E = 2.8\%$ in the first phase while later $\sigma_E = 2\%$). The asymmetric interval is chosen to maximize the $0\nu\beta\beta$ relative to $2\nu\beta\beta$ that has a steeply decreasing spectrum in this region. We then compute the number of $2\nu\beta\beta$ decay events left in each case. For the first phase we have 1.8 events $2\nu\beta\beta$ events left, while 5.5 events are left in the 100 yr ton data-sample. These backgrounds are then sta-

tistically subtracted using the $2\nu\beta\beta$ rate prediction from other regions of the energy spectrum. It should be remarked that on one hand this procedure relies on a good understanding of the resulution function, while, on the other, our total number of $0\nu\beta\beta$ events is conservatively estimated using the relatively short half-life predicted in [43]. The result in terms of sensitivities to the $0\nu\beta\beta$ half-life and neutrino masses are shown in Table 4, where the loss in efficiency due to the asymmetric cut (and to the tails beyond 2σ) are taken into account in the table as appropriate.

In summary this experiment at its various stages will allow us to explore neutrino masses in the range 10 meV - 1 eV, providing a unique opportunity for discoveries in particle physics and cosmology.

4 Xenon Enrichment Program

The isotopic enrichment of several tons of a heavy isotope represents a rather vast effort and, to our knowledge, it has never been attempted before, except for the case of (military and civilian) fissile materials. While the scale of the facilities employed for fissile materials is still a few orders of magnitude larger than what is needed here, it is quite clear that the main technical challenge for a very large $\beta\beta$-decay experiment is represented by the isotopic enrichment program.

Such enrichment could easily be performed at a military facility in Russia, providing at the same time a challenging program for the laboratory and its personnel. This program would naturally facilitate the transition towards other scientific and commercial enterprises within a healthy environment of scientific cooperation.

In the following sections we will discuss some of the issues related with the isotope enrichment program.

4.1 Enrichment Requirements and Techniques

The only isotope that can be used in our scheme is ^{136}Xe , a noble element in gaseous phase at standard conditions. ^{136}Xe also happens to be particularly easy to enrich (from the 8.9% content of natural xenon) using, essentially, any of the methods used for other isotopes. Xenon is completely non-reactive contrary to many other isotopes that are required to be combined in various chemical forms for separation, all stages of xenon handling are intrinsically safe.

Since in our case the purpose of the isotopic enrichment is to increase the amount of useful isotope inside the active volume of the detector, an extremely high level of enrichment is not particularly important. In the past ^{136}Xe $\beta\beta$-decay experiments have been performed with 63% isotopic enrichment and similar or slightly higher levels would be appropriate for this case.

The requirements on chemical purity of the Xenon are very stringent. This derives from two distinct issues. The large size of the TPC employed requires electron lifetimes in the gas of hundreds of μs. This can only be achieved if the concentration of electron scavengers like O_2, CO_2 and H_2O is sufficiently low. As discussed in a previous section such conditions are achievable through different steps of purification in the detector itself and do not depend directly on the quality of the isotopic enrichment process. Much more relevant here is the problem of radio-purity of the separated xenon. Although the detector will have superior background rejection capabilities, extreme care has to be taken in avoiding radioactive contaminants in the active gas volume.

As discussed later, raw xenon is generally produced from atmospheric air distillation where it is present at a concentration of 5×10^{-8}[46]. It is known that traces of ^{85}Kr ($T_{1/2}$ = 10.7 yrs) and ^{42}Ar ($T_{1/2}$ = 33 yrs) are present in the atmosphere since the advent of nuclear reactors and atmospheric testing of nuclear weapons. In

addition it is likely that the equipment used for the ^{136}Xe enrichment had processed uranium isotopes (probably in the form of UF_6) in the past. While U compounds can in principle be removed chemically after the isotopic separation, this cannot be done for Ar and Kr that, like Xe, are noble gases. However it has been shown [47] that, at least using ultracentrifugation, noble elements (and of course also U compounds) can be extracted from the xenon in a last step tuned for this purpose. This can be easily achieved because of the big mass difference between Ar, Kr, U and Xe. Presumably similar results can be obtained with most other enrichment techniques.

While Xe can be enriched with any known process, we will discuss here mainly the process of centrifugation that is in general considered to be the best suited for the purpose. In the past ^{136}Xe has been enriched in a single pass through a large centrifuge at Oak Ridge National Laboratory from the natural assay of 8.95% to 63.1% [48]. In an ultracentrifuge, see Figure 11, a cylindrical hollow rotor spins at

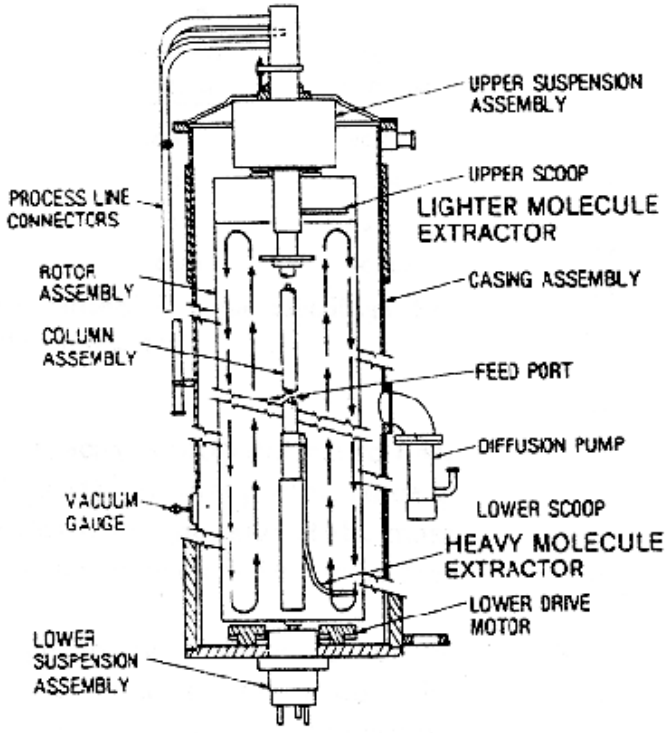

Figure 11: Cross section of an ultracentrifuge (from [48]).

very high velocity inside a high vacuum casing. Gas is fed half-way along the height of the rotor and is made convect by thermal gradients as indicated. In a fast centrifuge at regime the gas is mainly concentrated in small layers at the periphery of the rotor and near the central shaft. The difference in centrifugal force enriches the peripheral

layer of heavier molecules. The axial convective motion (that is typically orders of magnitude slower than the radial one) deposits preferentially heavy molecules in a lower scoop, and light molecules in a upper scoop. The ratio of flow-rate at the top extractor to the feed rate is usually referred to as "cut". The size, speed and setting of the centrifuge allow to place a cut in mass number extracted at the two ends. Often some mechanical modification or a slower feed rate are needed when processing gases much lighter than UF_6, since they tend to leak into the casing-rotor space increasing the drag and, ultimately, stopping the centrifuge. At mass 136 this effect is minimal and easy to correct.

While the United States abandoned its ultracentrifuge program in 1985, large plants using this technique exist at least in Russia and in Europe. Although our program will have to be developed with a Russian laboratory, we have investigated production and price issues with URENCO that runs a commercial production plant for stable isotopes in Almelo, Holland. Their preliminary price for enrichment in centrifuge cascades that are smaller than the US types but larger than the Russian, is shown in Table 5. These prices concern only the enrichment process. It is clear

Fraction of ^{136}Xe (%)	Amount of feed (tons)	Cost of ^{136}Xe (M$/ton)	Production time (years)
35	6	4 - 5	3
65	11	7 - 8	5
85	16.3	23 - 25	5

Table 5: Estimate of the enrichment cost *only* for ^{136}Xe . Prices are referred to one ton of *enriched* product and ultracentrifuge cascades are used.

from the table that the cost (that is crudely proportional to the running time) grows steeply with the enrichment grade required as well as with the amount of feed that one is willing to use in the process. A careful cost optimization will have to be performed to identify the best enrichment strategy given the technique and components used. The price of production at a Russian laboratory will have to be investigated from this starting point.

While in practice separation by gas diffusion is excluded since it would probably involve the engineering of new membranes for the purpose, enrichment by distillation and electromagnetic techniques (calutrons) would certainly be possible, and, albeit probably more expensive, it could present other advantages. Finally, laser separation could equal (and probably surpass) the economic and technical convenience of ultracentrifugation. However it is unclear to us whether a facility of the appropriate size exists in Russia.

Since the price of natural xenon is rather substantial (about $800k/ton in large quantities) the depleted isotope mix at the end of the separation process ($\sim$ 90%)

will have to be bought back by the xenon vendor. This is a standard procedure in the field. In fact even the ^{136}Xe fraction used in the experiment can be recovered and re-sold after the completion of the project. So in reality the only cost for xenon itself would correspond to the financing for 5 to 10 years of a value of ~$800k/ton.

It is also likely that a large fraction of the xenon needed could be obtained on loan from various Russian civilian laboratories. To our knowledge ton-quantities of natural xenon are available at least at ITEP (Moscow) (liquid Xe bubble chamber) and Novosibirsk (liquid Xe calorimeter development). We are at present investigating this issues in order to prepare an inventory of the material available.

Industrial xenon is mainly produced by air distillation [46]. In general Xe and Kr are collected together from large plants that supply liquid oxygen for metallurgical factories or produce generic gases for the industry. The mixture obtained contains 93% Kr and 7% Xe and the two gases are separated in special purpose distillation columns. The world xenon market has substantially expanded in recent times due to a relatively large demand for light bulbs and, most recently, Xe-ion rocket engines that require unprecedented amounts of the gas. Countries of the former Soviet Union and, in particular, Ukraine, are large producers, with 2,500 m^3 (STP) equivalent to about 14 tons in 1991, and a projected increase to 17 tons/year [49] in 1992 and 1993. The present world production of xenon is of several tens of metric tons per year and is increasing steadily with the demand.

Irrespective of the amount of xenon that can be obtained from Russian laboratories the above figures show that the ultimate size of the detector (10 ton ^{136}Xe), established above on the basis of the background requirements and available technology, matches reasonably well the industrial xenon production limits. 10 tons of ^{136}Xe are equivalent to about 100 tons of natural xenon to be processed (and 90% of it returned to the market). Apart from financial considerations, a further scaling by a factor of 10 (a 100 ton ^{136}Xe detector) would probably be impossible.

In general it appears that an enrichment (and detector construction program) able to process 10 tons of ^{136}Xe in about 5 years would be feasible and would match well the availability of feed stock.

4.2 Nuclear Non-proliferation Issues

The existence of large enrichment facilities with their support infrastructure and personnel in Russia poses a number of security and nuclear non-proliferation issues in todays volatile situation [50].

First, the economic situation of such laboratories is extremely poor and often even the minimum support needed to insure proper safekeeping of sensitive materials and components is not available. This poses a threat of theft that is not just hypothetical, as demonstrated by the alarming number of incidents reported since the collapse of Soviet Union [51].

Second, the lack of funding for such laboratories deeply affects the life of the highly

qualified engineers and scientists employed. Such personnel is forced to survive with severely insufficient salaries in an intellectual environment that is the shadow of the original one. Of course such conditions fuel temptation to desert to better paid and funded activities into countries that are secretly pursuing their nuclear ambitions.

Both these problems contribute to a frightening risk of nuclear proliferation, with small and unstable countries as well as well-organized terrorist groups potentially able to procure essentially unlimited amounts of fissile materials and highly skilled personnel to fabricate more or less sophisticated nuclear weapons. Indeed it should be assumed that if such a program can be carried-on from a technical stand-point it *will certainly* be enacted given a sufficient amount of money and time.

A complete solution to such proliferation threats has to occur through a gradual re-conversion program that addresses at the same time *both* the issues mentioned above. In fact each of the two problems (safekeeping and personnel) poses, by itself, very substantial proliferation risks. While it can be claimed that the problem of re-conversion from military to civilian activities is somewhat similar to the one encountered by US weapon laboratories in the past several years, none of the two issues mentioned above was a real concern in the US case. Furthermore Russian administrators have to face the extra burden of having to understand and adapt-to the market economy that will ultimately dictate the survival of a civilian laboratory in the global world market.

On a different front, while great progress has been made towards a situation of mutual trust and open facilities, the poor knowledge of installations and functions, hampers, particularly for some laboratories, the ability to help the reconversion.

We believe that the xenon enrichment program needed for this large double-β decay experiment can only be carried-on at one or more Russian laboratories and would, at the same time, naturally and effectively address all the non-proliferation issues described. The unprecedented size of this project represents a qualitative advantage. Although it is hard at this point to precisely asses the size of this enrichment program compared with the production capability of a Russian military laboratory, it is likely that such a project would provide revenues to support a non-negligible fraction of people and equipment, while allowing, if deemed appropriate, for the decommissioning of the bulk of the military production facility.

A program geared towards the production of 10 tons of ^{136}Xe would extend over a period of few years, providing the necessary stability for other re-conversion efforts. The relatively extended time period could also be utilized to gradually transfer to the laboratory, or a private venture associate to it, more responsibility for the project, that initially could be administrated through a western institution.

Equally important is the intellectual motivation of a program that, in terms of size and theme, is probably the closest possible approximation to the original mission of the laboratory. The ^{136}Xe enrichment would ideally match the expertise of the scientists and engineers involved, providing a stimulating and worthwhile working environment. The challenge of solving the technical problems for this large program

would over time gradually shift into the issue of improving the commercial return.

While the radio-purity requirements for this program would naturally require strict quality control and serve as training towards further commercial ventures, future large programs for isotope separation would naturally match and encourage the current increase of demand for applications in fundamental science, medicine and technology.

Besides the scientists and engineers involved in the isotope separation the project has been enthusiastically embraced by Russian civilian scientists at ITEP (Moscow) who have a long standing interest in the physics of $\beta\beta$-decay and in liquid and gaseous xenon ionization chambers [52]. We expect that other civilian laboratories in Russia and elsewhere will join our effort.

Initially we expect the involvement of non-government western scientists to be a very effective way of bridging the gap between the need of certain laboratories for support and their reluctance to enter a commercial partnership with a former foe. Later-on such collaboration among US, European and Russian scientists, accustomed to successfully work together in fundamental science, would function as a catalyst for involving the colleagues from the Closed Cities into a civilian research and development program. This environment would provide a constructive base for future endeavors directed towards the improvement of world security through the transformation of weapon facilities into healthy centers of civilian science and technology.

5 Acknowledgments

We would like to thank Prof. U. Becker (MIT), Prof. F. Boehm (Caltech), Prof. S. Drell (SLAC), Mr. H. Henrikson (Caltech), Prof. T. Neff (MIT), Dr. L. Ropelewski (CERN), Dr. G. Sher (CRDF), Dr. N. Smorodinskaya (CRDF and ITEP), Dr. R.W. Solarz (LLNL), Dr. A.J. Szady (ORNL), Mr. T. Thurston (SLAC) and Prof. R. Zare (Stanford) for many useful discussions.

References

[1] K.S. Hirata *et al.* (Kamiokande collab.) Phys. Lett. B205 (1988) 416;
K.S. Hirata *et al.* (Kamiokande collab.) Phys. Lett. B280 (1992) 146;
D. Casper *et al.* (IMB collab.) Phys. Rev. Lett. 66 (1991) 2561;
R. Becker-Szendy *et al.* (IMB collab.) Phys. Rev. Lett. 66 (1991) 2561;
W.W.M. Allison *et al.* (Soudan II collab.) Phys. Lett. B391 (1997) 491;
Y. Fukuda *et al.* (Super-Kamiokande collab.) Phys. Lett. B433 (1998) 9.

[2] C. Athanassopoulos *et al.* (LSND collab.) Phys. Rev. Lett. 81 (1998) 1774;
C. Athanassopoulos *et al.* (LSND collab.) Phys. Rev. C58 (1998) 2489.

[3] B.T. Cleveland *et al.* Astrophys. J. 496 (1998) 505;
M. Cribier *et al.* (Gallex collab.) Nucl. Phys. Proc. Suppl. 70 (1999) 284;
D.N. Abdurashitov *et al.* (SAGE collab.) Nucl. Phys. Proc. Suppl. 70 (1999) 299;
Y. Fukuda *et al.* (Kamiokande collab.) Phys. Rev. Lett. 77 (1996) 1683;
Y. Fukuda *et al.* (Super-Kamiokande collab.) Phys. Rev. Lett. 81 (1998) 1158, Erratum ibid. 81 (1998) 4279.

[4] Y. Fukuda *et al.* (Super-Kamiokande collab.) Phys.Rev.Lett. 81 (1998) 1562.

[5] P. Alivisatos *et al.* (KamLAND design report), Stanford-HEP-98-03, Unpublished;
W. Fulgione, to appear in Proceedings of Neutrino 98, Takayama, Japan, June 98.

[6] L. Wolfenstein, Phys. Rev. D 17 (1978) 2369;
S.P. Mikheyev and A.Yu. Smirnov, Sov. J. Nucl. Phys. 42 (1985) 1441.

[7] M. Apollonio *et al.* Phys. Lett. B420 (1998) 397.

[8] G. Gratta (for the Palo Verde Collaboration) in proceedings of WIN99, Cape Town, South Africa, Jan 99, World Scientific.

[9] M. Moe and P. Vogel Ann. Rev. Nucl. Part. Sci. 44 (1994) 247;
M. Moe Int. J. Mod. Phys. E2 (1993) 507;
F. Boehm and P. Vogel in "Physics of massive neutrinos" Chapter 6, Cambridge Univ. Press, 2nd Edition, 1992;
M. Doi, T. Kotani and E. Takasugi Prog. Theor. Phys. 83 (Suppl.) (1985) 1;
W.C. Haxton and G.J. Stephenson Jr. Prog. Part. Nucl. Phys. 12 (1984) 409;
H. Primakoff and S.P. Rosen Rep. Prog. Phys. 22 (1959) 121.

[10] M. Hirsch and H.V. Klapdor-Kleingrothaus Prog. Part. Nucl. Phys. 40 (1998) 323;
M. Hirsch, H.V. Klapdor-Kleingrothaus and S.G. Kovalenko Phys. Lett. B403

(1997) 291;
M. Hirsch, H.V. Klapdor-Kleingrothaus, S. Kolb, S.G. Kovalenko Phys. Rev. D57 (1998) 2020.

[11] F. Boehm and P. Vogel in "Physics of massive neutrinos" Chapter 6, Cambridge Univ. Press, 2nd Edition, 1992.

[12] S.M. Bilenki *et al.* hep-ph/9907234, Jul 7, 1999.

[13] K. You *et al.* Phys. Lett. B265 (1991) 53.

[14] L. Baudis *et al.* Phys. Lett. B407 (1997) 219.

[15] S. Elliott *et al.* Phys. Rev. C46 (1992) 1535.

[16] H. Ejiri *et al.* Nucl. Phys. A611 (1996) 85.

[17] A.Sh. Georgadze *et al.*, Phys. Atomic Nucl. 58 (1995) 1093.

[18] A. Alessandrello *et al.* Phys. Lett. 433 (1998) 156.

[19] R. Luescher *et al.* Phys. Lett. B434 (1998) 407;
J.C. Vuilleumier *et al.* Phys. Rev. D48 (1993) 1009.

[20] A. DeSilva *et al.* Phys. Rev. C56 (1997) 2451.

[21] A. Staudt *et al.* Europhys. Lett. 13 (1990) 31;
A. Staudt *et al.* Phys. Lett. B268 (1991) 312.

[22] E. Caurier *et al.* Phys. Rev. Lett. 77 (1996) 1954.

[23] H.T. Wong *et al.* Nucl. Inst. Meth. A329 (1993) 163.

[24] C. Brand *et al.* Nucl. Instr. and Meth. A283 (1989) 567.

[25] See for instance "SLS series HV power supplies", Spellman online catalog: http://www.spellmanhv.com.

[26] For a general review on GEMs and other similar devices see: F. Sauli and A. Sharma, CERN-EP/99-69, to appear in Annual Review of Nuclear and Particle Science.

[27] C. Amsler *et al.* Nucl. Inst. and Meth. A396 (1997) 115.

[28] F. Sauli, "Principles of Operation of Multiwire Proportional and Drift Chambers" CERN Yellow Report 77-09, Geneva 3 May 1977.

[29] A. Bressani *et al.*, Budker Institute Preprint INP-98-59, Novosibirsk 1998.

[30] Y. Giomataris *et al.* "Fast Signals and Single Electron Detection with MICROMEGAS Photodetector", Jul 1999, Unpublished.

[31] J. Séguinot *et al.*, Nucl. Instr. and Meth. A323 (1992) 583; J. Séguinot *et al.*, Nucl. Instr. and Meth. A354 (1995) 280.

[32] I.B. Berlman, "Handbook of Fluorescence Spectra of Aromatic Molecules" Second Edition, Academic Press, New York 1971.

[33] V. Vuillemin *et al.*, Nucl. Instr. and Meth. A316 (1992) 71.

[34] "Handbook of Chemistry and Physics" D.R. Lide, Ed., 76$^{\text{th}}$ Edition, CRC Press 1995.

[35] P. Benetti *et al.*, Nucl. Instr. and Meth. A329 (1993) 361.

[36] L. Thompson *et al.*, "TPC Readout Using the Gas Electron Multiplier", presented at the International Workshop on Micro-Pattern Gas Detectors, Jun 1999, Orsay, France; F. Sauli, CERN-EP-TA1, Internal Report, Jul 29, 1999.

[37] P. Cennini *et al.*, Nucl. Instr. and Meth. A345 (1994) 230.

[38] M.K. Moe Phys. Rev. C44 (1991) R931.

[39] W.B. Atwood *et al.* Nucl. Inst. Meth. A306 (1991) 446.

[40] H. Dehmelt, Rev. Mod. Physics 62 (1990) 525.

[41] W. Neuhauser, M. Hohenstatt, P. Toschek, and H. Dehmelt, Phys. Rev. Lett. 41 (1978) 233.

[42] G. Gratta *et al.* Nucl. Inst. and Meth. A400 (1997) 456.

[43] J. Engel, P. Vogel, and M. R. Zirnbauer, Phys. Rev. C37 (1988) 731.

[44] M. Guenther *et al.* Phys. Rev. D55 (1997) 54.

[45] D. Dassie *et al.* Phys. Rev. D51 (1995) 2090;
R. Arnold *et al.* Z. Phys. C72 (1996) 239;
A. DeSilva *et al.* Phys. Rev. C56 (1997) 2451.

[46] C.R. Hammond, in "Handbook of chemistry and Physics" 76th Edition, p.4-33, CRC Press.

[47] E. Bellotti *et al.* Nucl. Inst. and Meth. B62 (1992) 529.

[48] W.L. Roberts Nucl. Inst. and Meth. A282 (1989) 271.

[49] P.K. Lebedev and V.I. Pryanichnikov, Nucl. Inst. and Meth. A327 (1993) 222.

[50] A survey of these issues can be found, for instance, in G. Allison *et al.* "Avoiding Nuclear Anarchy", MIT Press 1995.

[51] "Nuclear Weapon and Sensitive Export Status Report: Nuclear Successor States of the Soviet Union", A cooperative Project of the Carnegie Endowment of International Peace and Monterey Institute of International Studies, No. 2 (Dec 1994), pp 39-58;
A. Bolsunovsky and V. Menshchikov, "Nuclear Security is Inadequate and Outdated", *The Monitor: Non-proliferation, Demilitarization and Arms Control*, University of Georgia, Athens, GA, Feb 1995;
"Chronology of Reported Illicit Exports for 1993 and First Quarter 1994", in Carnegie Endowment of International Peace and Monterey Institute of International Studies, No. 1, (May 1994), pp. 29-40.

[52] V. Artemiev *et al.* Nucl. Inst. and Meth. A303 (1991) 309.